NASA CONTRACTOR REPORT

NASA CR-1

NASA CR-1530

THERMAL AND ELECTROMAGNETIC RADIATION FROM DUST STRUCTURES

by Sylven N. Cutler and Carl N. Klahr

Prepared by
FUNDAMENTAL METHODS ASSOCIATES, INC.
New York City, N. Y.
for

NATIONAL AERONAUTICS AND SPACE ADMINISTRATION • WASHINGTON, D. C. • MARCH 1970

NASA CR-1530

THERMAL AND ELECTROMAGNETIC RADIATION FROM DUST STRUCTURES

By Sylven N. Cutler and Carl N. Klahr

Prepared under Contract No. NASw-1374 by
FUNDAMENTAL METHODS ASSOCIATES, INC.
New York City, N.Y.

for

NATIONAL AERONAUTICS AND SPACE ADMINISTRATION

For sale by the Clearinghouse for Federal Scientific and Technical Information
Springfield, Virginia 22151 – CFSTI price $3.00

ABSTRACT

An experimental program was conducted to determine behavior of dust particles as possible structured arrays for thermal and electromagnetic radiators in the space environment. The materials employed have been in the forms of dust particles with masses of 10^{-8} gram, and long ultra-thin flattened strips. The important characteristic of these materials is their large surface area-to-mass ratio. This work has examined experimentally their pertinent parameters for a number of applications as space structures.

Thermal radiation to be expected from a dust radiator has been experimentally simulated using a high-temperature dust stream radiating to a low-temperature absorbing background. Graphite particles with a diameter range from 50 microns to 200 microns were heated in vacuum to approximately 800°C and a stream of these hot particles was projected through the vacuum volume representing the space background. Average dust particle temperature before and after the traverse through this region was noted. Comparison with the theoretical analysis shows good agreement, indicating that each particle radiates to free space. This is an important result since it implies that the advantage of the large surface area of small dust particles can be fully realized.

X-band radiation interacting with random metallic dust volume distributions and long thin metallic strip arrays was also measured. The experimental results have been compared with the theoretical prediction and the two are found to agree.

TABLE OF CONTENTS

LIST OF FIGURES

SECTION 1
General Considerations

1.1 Introduction

This report deals with the results of an experimental investigation into the properties of dust particles in configurations which may offer significant advantages for application to space structures. The investigation has been concerned with the interactions of these dust configurations with electromagnetic radiation. The materials employed have been in the form of dust particles with masses in the range of 10^{-8} gram, and long ultra-thin shapes such as flattened strips. The important characteristic of these special forms is their large surface area-to-mass ratio. In a previous investigation, advantages to be realized from the use of materials having this property in space structure device applications have been pointed out.[1] Methods of deploying dust structures in space have also been suggested. The work here has examined experimentally the pertinent parameters for a number of these applications. The areas of experimental investigation have been the following:

1. Thermal radiation properties of dust particles radiating from a high initial temperature to a space environment
2. Reflective properties of random distributions of dust particles for electromagnetic energy in the microwave range
3. Reflection properties of arrays of parallel strips of metallic conductors of finite length for electromagnetic energy in the microwave range. Such arrays are of interest as simulations of long ultra-thin dust particle shapes.

The following general results have been noted with regard to the importance of dust in the high-performance space structure applications:

First, the high surface area-to-mass ratio of dust particles can effectively provide an efficient low total mass thermal radiator for space engines. The thermal radiation experiments have confirmed the estimates made previously[1] for such thermal radiators and also the advantages to be gained from dust particle utilization for this application.

Second, microwave reflection from finite-length metallic strips, even as short as one or two wavelengths, can still be reasonably high, provided that the gaps between them are small compared to a wavelength. An important result of this observation therefore is that the individual ultra-thin strips forming an array reflector need not be long, continuous conductors but can be broken into individual particles. For some space applications this provides an important reduction in the structural design requirements.

Third, the microwave reflection of dust particle distributions is very low if direct interface reflection is examined. On the other hand, dust particle distributions form effective equivalent dielectric materials and as such permit super-large size low-mass microwave lenses, total reflective devices for waveguiding, and for reflectors which use the total reflection phenomena. These devices will thus possess the properties and advantages of dust structures.

The results of each of the experiments will be briefly described within the following paragraphs of this section. A more detailed description of the experiments and their results will be presented in later sections.

1.2 Results of Dust Thermal-Radiation Experiments

The thermal radiation to be expected from a dust radiator has been experimentally simulated using a high-temperature dust stream radiating to a low temperature absorbing background. Graphite particles with a diameter range from 50 microns to 200 microns were first heated in vacuum to approximately 800°C. A stream of these hot particles was then projected through the vacuum volume representing the space background. Average dust particle temperature before and after the traverse through this region was noted. For example, typical temperature difference was of the order of 60°C. Comparison with the theoretical analysis for this case shows fairly good agreement. Even though the dust stream was spatially dense, visibly forming a dense dark region of particles, the agreement with the theoretical results indicates that each particle radiates to free space. This is an important result since it implies that the advantage of the large surface area of small dust particles can be fully realized.

1.3 Results of Planar Array Microwave Reflection Using Ultra-Thin Short Conductor Strips

The x-band reflection from a series of discontinuous array reflectors was measured and compared with that of a perfectly conductive sheet. Such broken arrays can represent an ordered trajectory of long ultra-thin reflecting particles, which may be termed "dust needles". These dust needles have the large surface-to-mass ratio advantage of other dust particles. A microwave test range using two horns which could measure the relative power reflection from the arrays was used. Each of the arrays consisted of a regular planar arrangement of parallel strips of flat thin conductors. The conductors were 1/16 inch wide and of negligible thickness. The strips were oriented with their flat side coincident with the effective reflector plane and periodically spaced with a periodicity of 1/4 inch. The strips were of finite length, varying from two wavelengths down to less than 0.2 wavelength. Gaps between strips in the direction along their length varied between 1/25 to 1/4 wavelength.

The following results were noted. Unless the lengthwise gap is large, say $\lambda/4$, the effect of the finite size of the strips is to cause a reduction in reflection loss of the order of 4 db or less, even for strip lengths as small as $\lambda/2$. For a gap length of $\lambda/25$, strips even as small as 0.3λ still only give less than 3 db reflection loss. However, a gap which becomes as large as $\lambda/4$ causes a large reflection loss going from 6 db at strip length of 2λ to 11 db at a strip length of λ. Notable however, was the special $\lambda/2$ strip length which for all cases showed a large effective reflection even for the $\lambda/4$ gap length case.

It can therefore be stated that arrays of conductive strips can represent good effective reflectors even with small-length conductors. For space structures a trade-off between total reflector size and individual reflector conductive strip is

reasonable if such finite strips represent a structural constraint. Finite strip-size reflector loss can be compensated for by the larger total reflector area.

1.4 Results of Dust-Microwave Interaction

The interaction of X-band radiation with random metallic dust volume distributions has been measured. The experimental results have been compared with the theoretical prediction using multiple independent scattering theory and the two are found to agree. As a result the metallic dust volume distribution represents an equivalent dielectric material whose dielectric constant ϵ is given by the expression

$$\epsilon = 1 + 3\beta$$

where β is the loading factor or the fraction of the total volume occupied by the dust particles. This permits one to analyze any dust distribution in a standard way for its effect on microwave radiation. Thus voltage reflection and transmission coefficients as well as phase delay can be easily found for arbitrary distributions.

The experimental results were obtained in standard X-band waveguide with measurements of voltage reflection and insertion loss. The dust distributions were formed and suspended in a petroleum jelly medium which was then loaded into the waveguide test section. This permitted a controlled dust distribution of desired density and form which could maintain the particle dispersal indefinitely. Correction for the dielectric constant of the petroleum jelly carrier medium was made, giving the results indicated above for dust suspended in vacuum.

SECTION 2

Interaction of Microwaves With Random Dust Distributions

2.1 Dust-Microwave Interaction

In this section, the results of experiments on the reflection of microwave radiation from a volume containing a spatially random distribution of dust particles are given and compared with predictions using multiple independent scattering theory. This comparison is in good agreement and permits the replacement of a dust region having any geometrical configuration by an equivalent dielectric having the same geometric configuration. Microwave reflection and transmission devices using dust distributions are then easily designed.

As will be shown below, the equivalent dielectric constant of a metallic dust-loaded volume can be given by the relation

$$\varepsilon \approx 1 + 3\beta$$

where β, the loading factor, is the proportion of the total volume occupied by the dust particles. This relation holds for small β only, but for practical devices this is the domain of interest if the dust space structure advantages are to be realized. For example, if 10% of the volume is occupied by the dust particles, the equivalent dielectric constant is 1.3.

As a consequence of the above result, dust volumes with low loading factor β are poor direct reflectors of microwave radiation. For $\beta = .10$, the interface between semi-infinite free space and the semi-infinite dust laden space provides little more than 4% power reflection. On the other hand, when special considerations such as total reflection at dielectric interfaces are taken into account, dust particles can be made to provide efficient reflection of microwaves. This concept, along with the use of the dust as an equivalent refractive dielectric material, allows for

the design of many types of dust microwave antennas, lenses, waveguides, gratings, etc. A number of these will be described in a later section.

All of the special structure types mentioned can serve as basic devices for dust space structure components having the special advantages to be realized from such structures. These advantages are, briefly, low total mass for super-large structure size and structural integrity under severe conditions of thermal radiation, meteoroid impact, etc.

The dust particles in the experiments here are micron-sized metallic particles and are thus many times smaller than the wavelengths at microwave frequencies. The experiments were performed with x-band radiation. The dust spatial density was sufficiently high to provide many particles per wavelength. Each particle scatters an amount of energy which is proportional to the volume of the particle. The collective effect of many such scatterers is proportional to the total volume occupied by all the particles. For a low dust loading factor the total scattered energy is equivalent to that reflected from a dielectric material rather than a metallic one. The important point however, is that even though dust scatterers are randomly located throughout the volume, the coherent component of resultant reflected and transmitted waves is very large compared with the incoherent component. An estimate of the relative amounts of each component has previously been made in Reference 1. The experiments described in this report give the value of the VSWR for the coherent component obtained from an interface between a dust laden space and free space and relate this value to the equivalent dielectric constant.

2.2 Method of Experimental Measurement of Dust Reflection

The measurement of dust reflection is of the amount of coherent reflection of microwave radiation at a flat interface between a dust-free region and a dust-laden region of similar cross sectional geometry, the interface being perpendicular to the direction of the impinging radiation. At such an interface, if both regions are semi-infinite, or equivalently well matched, and if both regions are lossless, then a single reflection measurement is sufficient to determine the equivalent dielectric constant of the dust-laden region. The reflection propoerties of the interface can be related to the normalized input impedance at the interface looking into the dust-laden region. This input impedance in turn is related to the equivalent dielectric constant. If Z_{in} is the normalized input impedance, the voltage reflection coefficient Γ is

$$\Gamma = \frac{Z_{in}-1}{Z_{in}+1}$$

For the case of a medium of infinite cross section which has a relative dielectric constant ε, the input impedance at the interface for the TEM mode is $Z_o/\sqrt{\varepsilon}$ where Z_o is the free space characteristic impedance. The voltage reflection coefficient is thus

$$\Gamma = \frac{1-\sqrt{\varepsilon}}{1+\sqrt{\varepsilon}}$$

For a practical measurement, it is more convenient to use a standard X-band rectangular waveguide as the transmission line structure rather than the plane or TEM waves in infinite space. The lowest mode in rectangular guide has a characteristic impedance Z, with

$$Z = \frac{Z_o}{\sqrt{\varepsilon}} \frac{1}{\sqrt{1 - \left(\frac{\lambda}{\lambda_{c\varepsilon}}\right)^2}}$$

where λ is the free space wavelength, Z_o again the free space characteristic impedance equal to 377 ohms, and $\lambda_{c\varepsilon}$ the cutoff wavelength for the dielectric filled guide. $\lambda_{c\varepsilon} = \lambda_c\sqrt{\varepsilon}$ with $\lambda_c = 2a$ where a is the broad dimension of the waveguide. Putting $p = \lambda / \lambda_c$, the voltage reflection coefficient due to the impedance discontinuity at the interface in the waveguide is now

$$\Gamma = \frac{\sqrt{1 - p^2} - \sqrt{\varepsilon - p^2}}{\sqrt{1 - p^2} + \sqrt{\varepsilon - p^2}}$$

Again it has been assumed that the guide is well-matched and that only the lowest mode is present. In terms of the voltage standing wave ratio r, where $r = (1 + |\Gamma|)/(1 - |\Gamma|)$, the dielectric constant is given by

$$\varepsilon = p^2 + (1-p^2)\, r^2$$

where we can write $p = \lambda/2a$. Thus in the non-lossy case, the single measurement of r in the waveguide can serve to determine ε. If ε is complex, as it is for the lossy case,* the measurement is more complicated. However, the measurements of insertion loss in the actual experiments were sufficiently low to permit the use of the above formula as a good approximation.

---

* Loss may be caused by two mechanisms. First, loss may be due to the finite conductivity of the particles themselves, and may be large for poor conductive materials. Second, loss may be the result of the incoherently scattered component. This however, is small.

One assumption mentioned above used in the input impedance expression is that only the lowest rectangular waveguide mode is propagating so that the characteristic impedance for that mode can be used. This is assured in the empty guide simply by the use of x-band guide at x-band frequencies. However, the introduction of the dielectric filling the guide lowers the guide mode cutoff frequencies, each by the factor $1/\sqrt{\varepsilon}$ *. Since values of $\varepsilon \leq 2.0$ were determined (the result of the equivalent dust dielectric plus the carrier medium to be described later) and since the next higher mode cutoff above the fundamental mode for the unloaded guide is about 13 Gc/sec, the cutoff of the loaded guide for that mode would be close to 9.5 Gc/sec. Therefore great care was taken to avoid excitation of the higher order modes, both propagating and non-propagating, by avoiding any special irregularities in the geometry of the system other than the sharp interfaces.

A second assumption in the above discussion was that the guide was well-matched. This means that the inpud impedance at the interface could be taken as the characteristic impedance of the dust-laden guide and did not depend upon the length of the dust-laden guide test section or any guide components beyond the test section. While this is not absolutely necessary, since the reflections at both boundaries of a known finite size sample could be taken into acoount in the expression for the VSWR, it was more convenient to operate with an effectively semi-infinite test section (the well-matched section). One simple way of achieving such a match over a finite length of test sample was to gradually taper the dielectric

---

* The cutoff wavelengths for a dielectric-filled rectangular waveguide are given by

$$\lambda_{cmn} = \frac{2a\sqrt{\varepsilon}}{\sqrt{m^2 + n^2\left(\frac{a}{b}\right)^2}}$$

where m, n are the mode indices, a is the wide guide dimension, b the narrow guide dimension, and ε the dielectric constant of the material completely filling the guide

sample at one boundary or interface back to the unloaded guide. A matched load or any other matched components can then be used beyond the test section. If the taper is made long enough, little overall reflection occurs for the taper discontinuity and the system is matched. A schematic drawing of the test section is shown in Figure 1.

To assure that a good match with the taper was obtained, tests were first made on the VSWR due to the taper. Ragan [2] gives the VSWR expected from a taper of given length in a parallel plate transmission line. For a taper length-to-wavelength ratio of 1 or more the VSWR is better than 1.06. Similar considerations hold for the rectangular waveguide. At 9500 Mc/sec the free space wavelength is 3.15 cm and the wavelength of the guide (RG52/U) is 4.36 cm. In partially or completely dielectric filled guide, the guide wavelength is smaller. The taper test section used was 2 inches (5 cm) and therefore the taper-to-wavelength ratio was greater than 1. The taper test section was a dielectric loaded waveguide section with a similar taper at either end. The VSWR from such a section would be a function of the taper dimensions and the length of the completely filled section between the two tapers. By varying the section between the two tapers, it was found that the maximum VSWR attainable was always less than 1.08*. It could safely be concluded therefore that the single taper on the test section of Figure 1 would produce a mismatch with a VSWR of 1.04 or less. For practical purposes, the line can therefore be considered to be a matched one. Because of the nature of the carrier dielectric medium such sections could be made easily.

---

*If two impedance mismatches are present, each producing a VSWR of r separately, then the VSWR due to both in the line can vary between 1 and r^2 dependent on the length of section between the two.

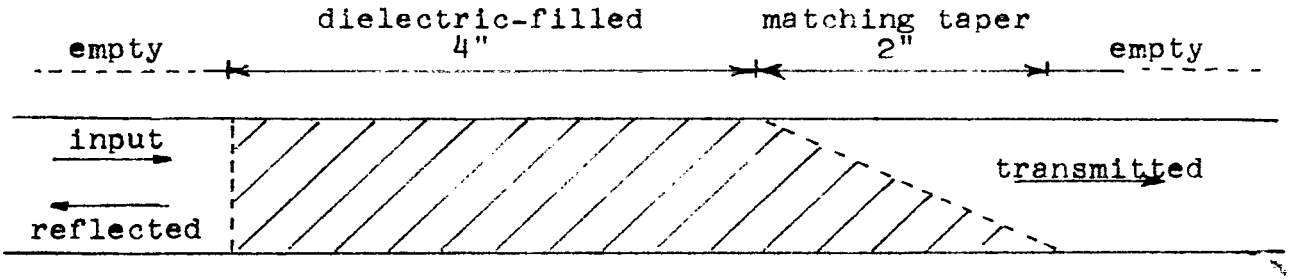

Figure 1. E Plane Section of X-Band Waveguide for VSWR Measurement from Dust Region-Free Space Interface

The final test sections for determining VSWR and insertion loss were made with a single taper and a flat interface (perpendicular to the axis of the guide) at the opposite end. The test bench schematic is shown in Figure 2. All measurements were made at 9500 Mc/sec.

A number of different designs of test sample structures were tried. For example, one was a suspension of dust particles in oil contained in a plastic box fitted to the inside of the waveguide walls. This however, suffered from problems of maintaining a uniform spatial distribution of particles during the test. In addition, extra approximations are required because of the plastic container walls.

The final, most practical, and extremely simple design was a suspension of particles in petroleum jelly (Vaseline). A proper mixture could be made, the waveguide completely filled without any irregularities such as large air bubbles, and the flat face or the taper formed with ease. Once prepared, the sample maintained its shape and the particles remained suspended indefinitely.

A uniform spatial distribution of dust particles with the desired spatial density could be made by mixing a specific weight of dust particles with a given volume of Vaseline. This mixture was mechanically stirred until a very uniform distribution resulted. Uniformity could easily be checked visually under the microscope. Furthermore, several different batches with the same ratios were made and checked electrically. These all resulted in the same experimental values. The test fixture which was filled with the mixture and shaped was a standard 6 inch length of RG52/U waveguide.

Comparison of the dust-laden carrier (Vaseline) had to be made with the same carrier without dust. This is so since the carrier has a dielectric constant greater than 1. The equivalent dielectric constant for dust distributed in vacuum can then be evaluated by determining the perturbation effect of the dust in the carrier compared with that for the pure carrier.

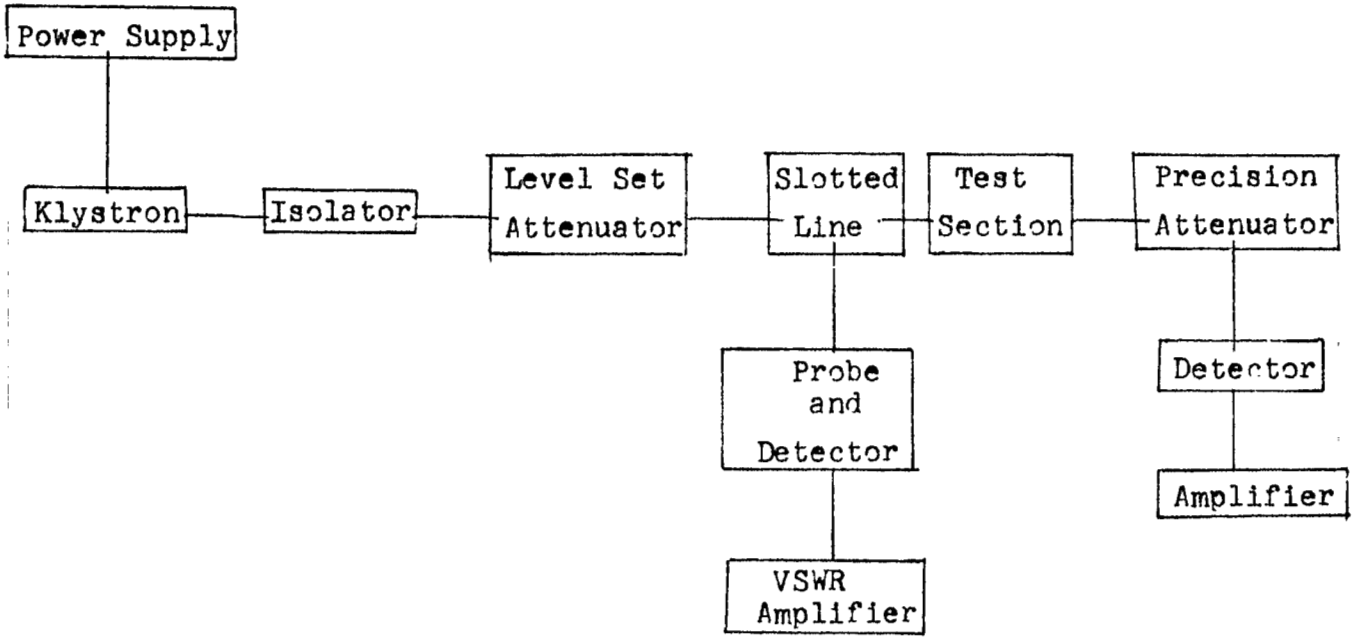

Figure 2. Experimental Test Bench for Determining Dielectric Constant of Dust Distribution in Waveguide

Von Hippel[3] gives the properties of Vaseline at 10^{10} cps as $\varepsilon = 2.16$ and $\tan \delta = 10^{-3}$. (Tan δ is the loss tangent.) The total length of sample was 4 to 6 inches. This length would provide less than 0.2 db loss with this loss tangent and therefore can be neglected.

The listed value of the Vaseline dielectric constant could not be used in the calculations. Obtaining a uniform distribution of dust throughout the Vaseline required stirring them together. This stirring introduced a distribution of very tiny air bubbles throughout the mixture, resulting essentially in an air-dust-Vaseline mixture. The standard carrier material which served as the reference was therefore Vaseline stirred sufficiently and in a similar manner as that used for the final dust mixture. The resultant bubbles were of small enough size and dispersed through the Vaseline with sufficient uniformity to provide a reasonable unloaded (free of dust) carrier standard. The actual measured dielectric constant of the carrier medium (air bubble-Vaseline mixture) was $\varepsilon = 1.5$. The loss was negligible, as expected.

2.3 Multiple Dipole Scattering by Dust Distributions

It is useful to apply the theory of multiple but independent scattering of electromagnetic radiation to the problem of dust distributions. The theory of molecular optics explains the dielectric constant of a medium as due to the scattering properties of the molecules. For such a problem, as well as in the present case, the range of interest is that for which the scatterers are very small compared to the wavelength of the radiation and also for which there are many such scatterers per wavelength. The scattering is then characterized by the polarizability for a single particle which is proportional to the field at that particle. Because of the small size of the particle compared to the wavelength, the exciting field can be taken constant over the particle region. The exciting field at any one particle is the total field due to the incident field plus that due to the scattered field from all the other particles. For large numbers of particles per wavelength the statistical effect of all the particles gives rise to the Lorentz-Lorenz formula[4] of molecular optics. This gives the relationship between the index of refraction $n = \sqrt{\epsilon}$ and the polarizability a single particle α as

$$4\pi\alpha N = \frac{3(n^2-1)}{n^2+2}$$

where N is the number of particles per unit volume, and for which the particles or scatterers are thought to be suspended in vacuum. n is real if the particles are lossless, which implies that α is real. This result would seem to indicate that there is no loss through a particle medium as long as the particle itself is lossless. However, even with perfectly conducting particles, the particle polarizability may have a small component out of phase with the incident radiation resulting in an overall lossy term. This however, is of higher order than those terms considered here and is not included in the approximation to the effective dielectric constant.

The Lorentz-Lorenz formula is derived assuming the excitation of an electric dipole only where the electric dipole is $\bar{p} = \alpha \bar{E}_o = a^3 \bar{E}_o$ where $\bar{E}_o$ is the exciting electric field, a the spherical particle radius, and α the polarizability. For a perfectly conducting particle, besides the surface charge giving rise to the electric dipole moment $\bar{p}$, there are surface currents which provide an equivalent magnetic dipole. The magnetic dipole has the value $\bar{m} = -\frac{1}{2} a^3 \bar{H}_o$ where $\bar{H}_o$ is the exciting magnetic field. The minus sign adds extra power into the backscattering angle. However, even if all particles are assumed to constitute electric and magnetic dipoles and then the resultant equivalent dielectric constnant for the random collector is evaluated, significantly different values of n from that above for reasonable dust densities are not obtained.

One fundamental correction is needed for the experimental results. It is the fact that if a similar formula should apply, note must be made that the scatterers are not suspended in vacuum but in a dielectric medium (in this case, Vaseline). A formula for this latter case can be derived and gives the following result (see Appendix I).

$$\varepsilon' = \frac{\varepsilon + \frac{8\pi}{3} N a^3 \varepsilon}{1 - \frac{4\pi}{3} N a^3 \varepsilon}$$

where ε' is the effective relative dielectric constant of the carrier-scatterer mixture, ε is the relative dielectric constant of the carrier, N is the number of scatterers per unit volume, and a is the scatterer radius. Here the scatterer has been taken to be a perfectly conducting sphere of radius a and the polarizability of the particle has been inserted in the formula.

Each dust particle is of small enough size compared with the wavelength and there are sufficient particles per wavelength to insure that the above result should hold true here.

2.4 Experimental Results for Dust Reflection

As described in Section 2.2, various amounts of powders were mixed into the petroleum jelly and loaded and shaped in the waveguide test section. The VSWR in each case was measured. Estimates of the loading ratio $(4\pi/3)(a^3N)$ were made and a comparison was obtained between the experimental value of the effective dielectric constant and that computed by the formula of section 2.3. Table 1 lists the experimentally-determined results for some typical cases.

Table 1

Measured VSWR for Various Dust-Vaseline Mixtures

Material	Weight Ratio (Material/Vaseline)	Loading Ratio $\frac{4\pi}{3} a^3N$	VSWR
Aluminum (20 μ diam.)	1/15	.02	1.95
Aluminum (20 μ diam.)	1/3	.10	2.50
Copper (20 μ diam.)	1/3	.03	2.10

The loading ratios were determined from the following considerations. The reduced density of the air-Vaseline mixture (the Vaseline after stirring without dust) as measured is $\rho = 0.8$ g/cm^3. Adding a mass of dust M_p to a given mass of Vaseline M_v (before stirring) gives a dust mass density of $(\rho/M_v)(M_p)$. The volume of the dust is small compared to that of the Vaseline and can be ignored.) The loading ratio $\beta = (4\pi/3)(a^3N)$ is then given by

$$\beta = \frac{\rho}{M_v} M_p \frac{1}{\delta}$$

where δ is the particle material density.

For each of the cases of Table 1, the value of the equivalent dielectric constant according to the theoretical formula of Section 2.3 and the experimentally determined values of Section 2.2 is given in Table 2.

Table 2

Equivalent Dielectric Constant for Dust in Vaseline

Material	Weight Ratio (Material/Vaseline)	ε' Theoretical	ε' Computed from VSWR
Aluminum	1/15	1.61	1.50
Aluminum	1/3	2.12	1.79
Copper	1/3	1.66	1.58

For purposes of computation in the theoretical formula, we note that ε for the carrier medium was measured as 1.5. As noted, the values of ε' in Table 2 are the overall effective dielectric constants for the air-Vaseline-dust mixture.

Values are in fairly good agreement and would indicate that the formula according to the Lorentz-Lorenz equation can be used here with a fair degree of accuracy. It is thus possible to use this same formula with $\varepsilon = 1$ corresponding to the suspension of dust in vacuum. Letting β equal the dust loading factor, i.e., $\beta = (4\pi/3)(Na^3)$, the dielectric constant is given by

$$\varepsilon' = \frac{1 + 2\beta}{1 - \beta}$$

For $\beta << 1$, this gives $\varepsilon' \approx 1+3\beta$ as indicated in Section 2.1.

2.5 Application of Volume Dust Distributions as Space Structure Microwave Devices

It has been noted that there is good agreement between the experimentally determined reflectance of dust distributions and the theory which assumes multiple independent scattering from the dust particles. For this result, each particle acts as an induced dipole with a polarization proportional to the particle volume which is extremely small in this case. A practical large reflectance would require a large quantity of dust, much larger than is desired if the advantages of dust structures are to be realized. However, even with this restriction, useful microwave devices with low dust density can be achieved if advantage is taken of the equivalent dielectric properties of dust distributions. A partial listing of these includes the following: large microwave lenses, waveguides, and even reflectors (if the concept of total reflection at dielectric interfaces is used).

A dielectric lens for example, can be used to focus microwave power. Typical lenses of solid materials are made of dielectrics such as plexiglass with a refractive index of 1.6. These are limited in size however, because of the large thicknesses of material required and the resulting problems of manufacture and integrity. As a result, zoning is often employed to reduce the physical thickness but such devices suffer from problems of frequency sensitivity. Dust distributions as space structures thus offer the possibility of extremely large, low mass, microwave lenses. These could be used as single lenses for focussing of a microwave beam, as an element in a periodic array for a quasi-optical transmission line, etc. Other applications could include the formation of lenses with spatially-varying dielectric constant for devices like the Luneberg lens and many others.

A crucial point of course is the tolerance requirement placed on any lens.[5] Criteria place upper limits in the irregularities of the wavefronts resulting from irregularities of the surfaces or dielectrics. This corresponds normally to $\lambda/16$ which implies a thickness tolerance of

$$\Delta t \leq \frac{\lambda}{16\,(n-1)}$$

and an index tolerance of

$$\Delta n \leq \frac{\lambda}{16\,t}$$

where t is the thickness, λ the wavelength, and n the index of refraction. For example, a loading factor $\beta \approx .1$ as indicated above gives $n = \sqrt{\epsilon} = 1.14$. Therefore, at 3 cm radiation, $\Delta t \leq 1.35$ cm. Obviously the technique of forming and maintaining a dust lens in space is a critical point.

The dust space structures which can be used as waveguides and antennas in the microwave range use the principle of total reflection at dielectric interfaces rather than metal conductor reflection. All dielectric material waveguides can be formed using this principle.[6] If an inner dielectric, whose dielectric constant is ϵ_1, has an outer cladding whose dielectric constant is ϵ_2 and if $\epsilon_1 > \epsilon_2$, then total reflection can occur for angles of incident radiation in the higher value dielectric, where $\sqrt{(\epsilon_1/\epsilon_2)}\,(\sin\theta) > 1$. Here θ is the angle of the incident radiation relative to the normal to the interface. Waveguides can be constructed using this principle providing the propagating mode represents angular reflections within this limitation.

The outer cladding in principle is not needed for total reflection since free space has $\epsilon_2 = 1 < \epsilon_1$ for any dielectric. However, the cladding is often used to control the propagating

modes (angles greater than θ) as opposed to the non-propagating or radiating modes. The restriction for a slab waveguide with inner dielectric ε_1 and outer cladding ε_2 to support a propagating mode is that

$$\frac{d}{\lambda}\sqrt{\varepsilon_1-\varepsilon_2} \geq \frac{m}{2}$$

where d is the width of the inner dielectric, λ the wavelength, and $m = 0$ or an integer[7]. For a given value of m, all modes with a mode order $n \leq m$ will propagate and modes with mode order $n \geq m$ will represent a leaky mode and radiate from the structure. There is no restriction on d and so this can represent structures many wavelengths wide. Thus if only the lowest TE and TM modes are to propagate, i.e. $n = 0$, one can choose $m \simeq 1$ to determine the parameters. Therefore $\Delta\varepsilon \geq (\lambda/2d)^2$. For example, with $d/\lambda = 10$ one needs $\Delta\varepsilon \geq .0025$, a very difficult restriction on the tolerance of the outer cladding material if formed from dust. On the other hand, if one allowed a highly over moded guide, say $m = 10$, then $\Delta\varepsilon \geq .25$ which with $\varepsilon_1 = 1.3$ corresponds almost to no outer cladding. The propagating mode is then determined by the excitation pattern and any irregularities exciting the other modes.

As the ratio between the inner and outer dielectric constants becomes larger, angles closer to the normal can also result in total reflection. Therefore more modes become propagating modes rather than leaky ones. Considered from the point of view of the field across the guide, the propagating mode has an exponential decay outside the dielectric structure.

The dielectric slab waveguide described above consists of an inner core material and an outer cladding. The entire propagating structure is dielectric. A different version is the hollow

dielectric structure which can have a similar kind of mode structure with only a thin shell dielectric[6]. Here free space forms the outer cladding at which total reflection occurs. Propagation is confined essentially to the inner vacuum region and the dielectric shell. A diagram of the totally reflecting dust waveguide is shown in Figure 3. The energy is essentially bound to the dielectric with an exponential field decay outside the dielectric and a hyperbolic variation in the inner vacuum region.

These dielectric waveguide structures can be used in a number of ways. First they can be used as ordinary transmission lines. On the other hand, antenna structures can also be fashioned from them. Proper choice of equivalent dust dielectric, thickness, size, and shape can result in a leaky wave which thus forms a traveling wave antenna. Alternatively, propagating non-leaky waves can be made to radiate from a series of slots or holes in the dust wall forming the dielectric. Finally, the guide can be open directly at one end or flared gradually to an open end to form a radiating horn.

A completely different type of antenna structure is also possible based on the principle of total reflection. The dust distribution can be placed in the shape of a truncated parabola (vertex zone removed) with the condition that the angle of incidence of the radiation from the feed to the surface is such as to suffer total reflection as shown in Figure 4. The structure need only be a thin shell with the ray refracting through the first interface between vacuum and the dust layer and being totally reflected at the back surface. After the first totally reflected ray at the outer interface it is necessary to avoid a second total reflection at the final dielectric-air surface before emerging parallel to the parabola axis. To do this the dust density of the parabolic shell should be tapered gradually to zero on the focal side of the shell. Thus only one total reflection occurs at the outer interface. For the two dimensional case with a parabola given by $y = 2px$, and the feed along the axis at $x = p/2$, all parts of the parabola satisfying the condition

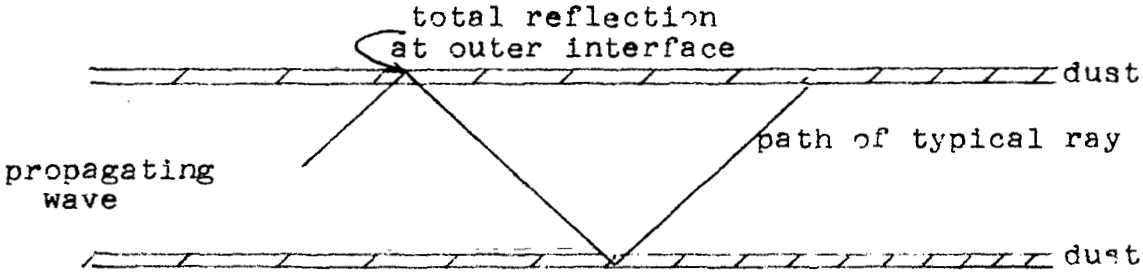

Figure 3. Dust Dielectric Waveguide

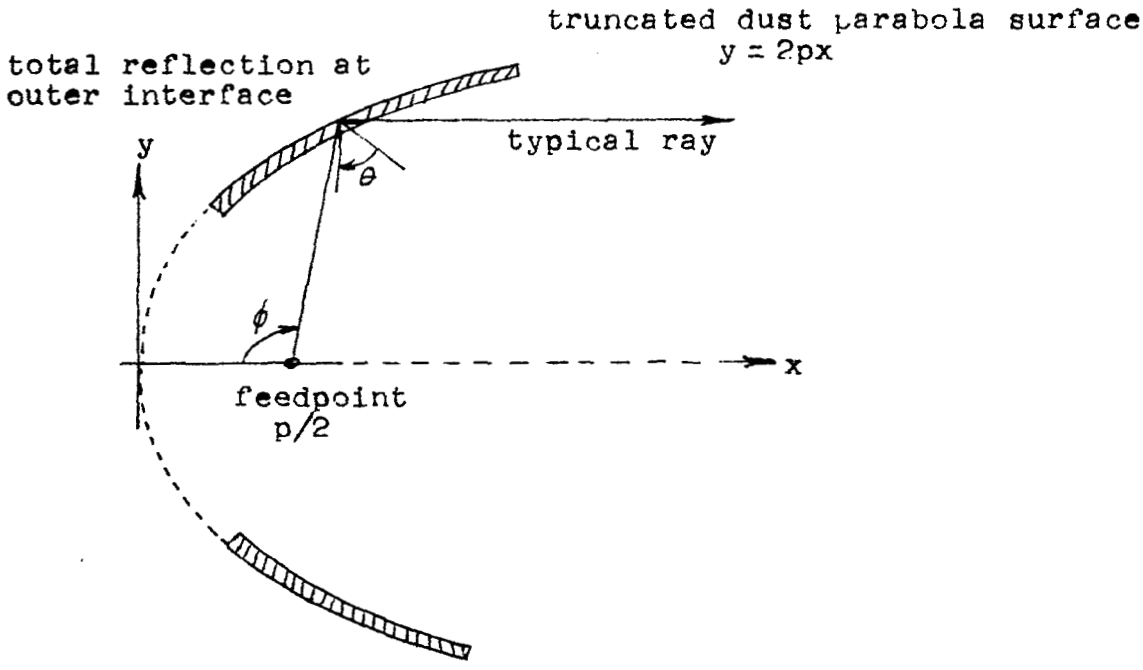

Figure 4. Truncated Parabolic Reflector Constructed of Dust

$$x \geq \frac{2p}{\varepsilon_1}\left(1 - \frac{1}{\varepsilon_1}\right)$$

could meet the condition of total reflection. (Here the change in angle due to refraction at the first interface has been neglected. For $\varepsilon_1 = 1.3$ this gives $x \geq .36p$. The remainder of the parabola could be made as large as desired. The truncated portion would result in some decrease in gain and higher side-lobe level but this may still be acceptable. Numerous other structures using total reflection for antenna devices in single and array devices are also possible.

It is thus evident that while the dust distribution can not be used as a reflector for normal incidence, lower angle incidence, resulting in total reflection offers many possibilities for device design.

SECTION 3
Reflection of Microwaves from Planar Arrays of Short Metal Strips

3.1 Planar Array Reflection of Microwaves

The advantage of large surface-to-mass ratio is not confined to spherical particles; it is even more pronounced for long filamentary needles, so long as the cylindrical radius is small. There are a number of materials which can be conveniently fabricated in the form of long thin whiskers, needles or filaments. Such "dust needles" can then be projected or circulated in space in such a way that their relative orientation is maintained. In this form a dust needle array has a much larger microwave reflection coefficient than a disordered collection of dust particles. In this section we shall investigate the reflection properties of such an array.

The planar array of conductive wires or strips of arbitrary cross section can, under the right conditions, serve as a microwave reflector equal to that for a solid sheet conductor. These conditions, which are well-known and find application in practical devices, are the following: First, that the wires should be oriented parallel to the incident electric field, second, that the wires be many wavelengths long, and third, that there be many wires per wavelength or equivalently, that the spacing between wires be small compared to a wavelength. Thus a grid of parallel, very thin wires can serve as a perfect reflector if spaced closely enough and oriented parallel to the electric field, even though the percentage of effective reflector area covered by metallic material is very small.

The equivalent circuit for a regular planar array for which the wires are infinitely long and periodically spaced has been evaluated in the past and is given in standard texts, notably "The Waveguide Handbook"[8]. Further, this can be given for arbitrary orientation of the incident plane wave. For the purpose of reference, the equivalent circuit for two special cases is given in Appendix II. The equivalent circuit permits the calculation of the reflection and transmission coefficients very easily.

On the other hand, arrays other than the special types given in the handbook are difficult to treat and generally involve either a very rough approximation procedure for the equivalent circuit or an experimental investigation for each type of array. One type of such an array has been examined here. This is the periodic array of strips with gaps placed or cut out along their length. This results in an array of finite-length conductors, the length being of the order of a wavelength or smaller. The importance of such arrays is to determine if and how quickly the reflection properties of wire arrays decrease if the wires are not long or are broken in some manner. The investigation is restricted to the case of the incident electric field oriented parallel to the original long dimension of the strips. Figure 5 shows a diagram and notation for the planar arrays tested.

Certainly one can easily believe that if the remaining strips after cuts are made are still long compared with the wavelength and the gaps are small compared with a wavelength, then little change should be noticed from the uncut array. However, as either the strips become shorter or the gaps longer, the amplitude of the reflected wave is expected to be reduced.

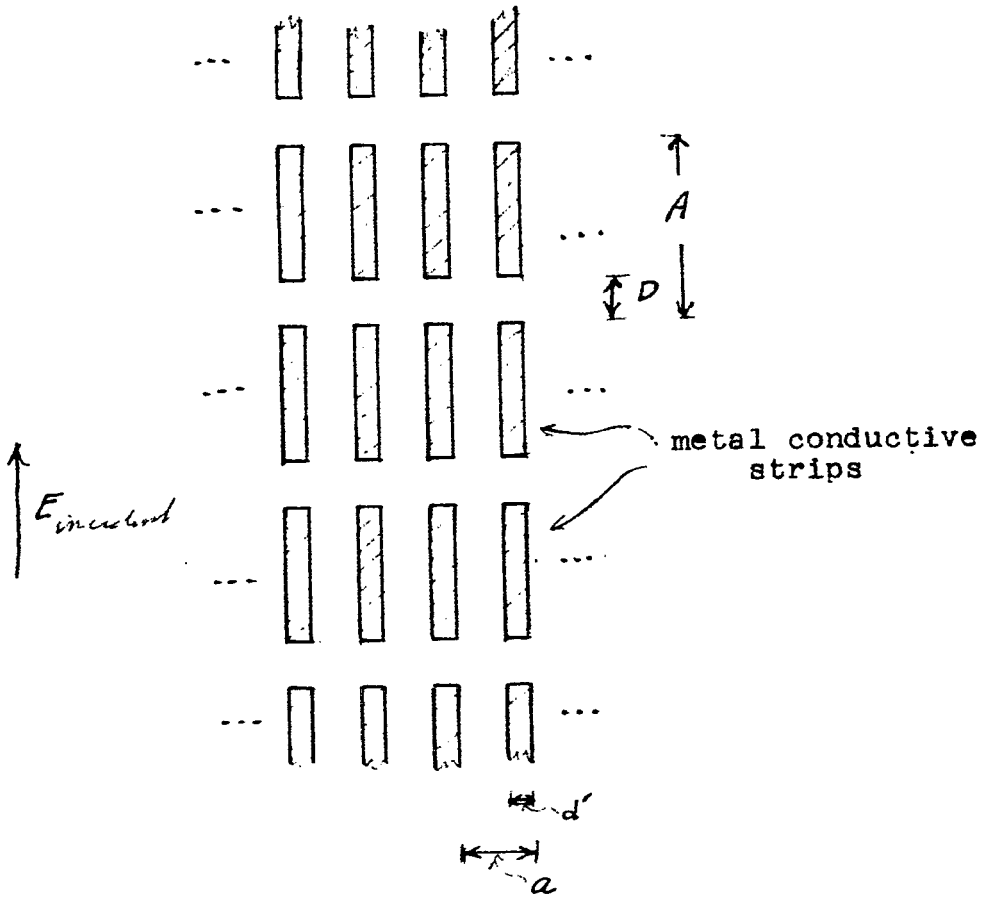

Figure 5. Planar Array Test Pattern

This is fairly evident. The question of how rapidly the fall-off of the reflective coefficient occurs is not. Furthermore, there may be special geometrical ratios of the remaining conductive elements for which resonances occur with greatly increased or decreased transmission or reflection much as is the case for special size apertures or irises in waveguides.

A number of reflection experiments have been conducted on the cut periodic strip planar array. These will be described below. The results show that such arrays of small-size strips can also be useful as reflective planes if some small decrease in reflectance can be tolerated. Strips one or two wavelengths long suffer only a few db reflection loss if the gap is small compared to the wavelength. For space structures with super-size elements, a tradeoff between the higher gain of the extra large antenna and the reduced reflection of the small but more convenient shorter wire conductors might be of importance.

3.2 Reflection Measurement Methods for Planar Arrays

Reflection measurements were made on a number of planar arrays of the type shown in Figure 5 at a frequency of 9500 Mc/sec. The radiating antenna was a small rectangular tapered horn with and E-plane aperture of 1.25 inch and an H-plane aperture of 1.75 inch. Using an E/H tuner for matching, the VSWR of the horn looking into free space was better than 1.08. A similar horn was used as a receiving antenna which was also matched to better than 1.08 VSWR. Since measurements were made on a wide range of reflectors, in some cases resulting in reflected power at least 30 db down from a perfect reflector, it was necessary to avoid non-linearities in the detector circuit. Therefore a precision attenuator was placed in the receiver circuit and adjusted in each measurement so that the received signal was the same for all arrays. Also the db change in reflected power could be read then directly on the attenuator.

The far field of the horns began at about 7 inches from the aperture. The array panels were placed 10 inches from the horns. Microwave absorber material was placed behind the panels and at any other positions where spurious reflections might be troublesome. The receiver horn was placed directly above the horn and the panels angled with the normal to the panel bisecting the angle of the transmitter-receiver alignment as seen from the panel. This placed the maximum of the return beam at the receiver horn for the perfect reflector. As explained later, the finite size of the test panels formed a multi-lobed return signal. A uniline in the transmitter circuit prevented the transmitter from being affected by a portion of the return signal from the reflector. Multi-reflections for panel side lobes between the various elements of the system were not found to be a problem.

Direct coupling between the two horns was down at least 60 db as compared with the perfect reflector panel signal. The H and E plane patterns of the horns were measured and found to agree with theory. Thus the 10 db full beam width for the horn should be $87\frac{1}{2}^{\circ}$. The measured value was 90°. Figure 6 shows the schematic diagram for the experimental range.

A reflecting rectangular panel of finite size (in this case 11 inches by 11 inches) has a multi-lobe structure similar to that for any illuminated aperture of the same overall size. For uniform illumination, the first minimum is at $\theta \approx \lambda/H$ where H is the panel linear size. In this case this corresponds to approximately 6°. With tapered illumination, as is actually present with the horns and spacing used, the amplitudes and positions of the lobes change. For example, with a cosine squared illumination, the first minimum shifts to $2\lambda/H$. Phase variations in the illumination also cause a change in the lobe structure. An odd phase variation over the panel shifts the main beam itself. Care was taken to provide an even illumination by keeping the panel and horn arrangement centered to avoid phase errors. A test of the solid conductive sheet showed a lobe structure as predicted, with the given illumination.

The measurement of the reflecting power of any array was made by comparing the magnitude of the main lobe for each array with that of a standard, perfectly reflecting metal plate of the same size and shape, i.e., rectangular solid sheet conductor 11 by 11 inches, as the array panels under similar experimental conditions. Thus for a perfect reflector of effective area A at a distance R, incident power P_o, and antenna gain G, the reflected power is

$$P_r = \frac{P_o G}{4\pi} \frac{A'}{2R^2}$$

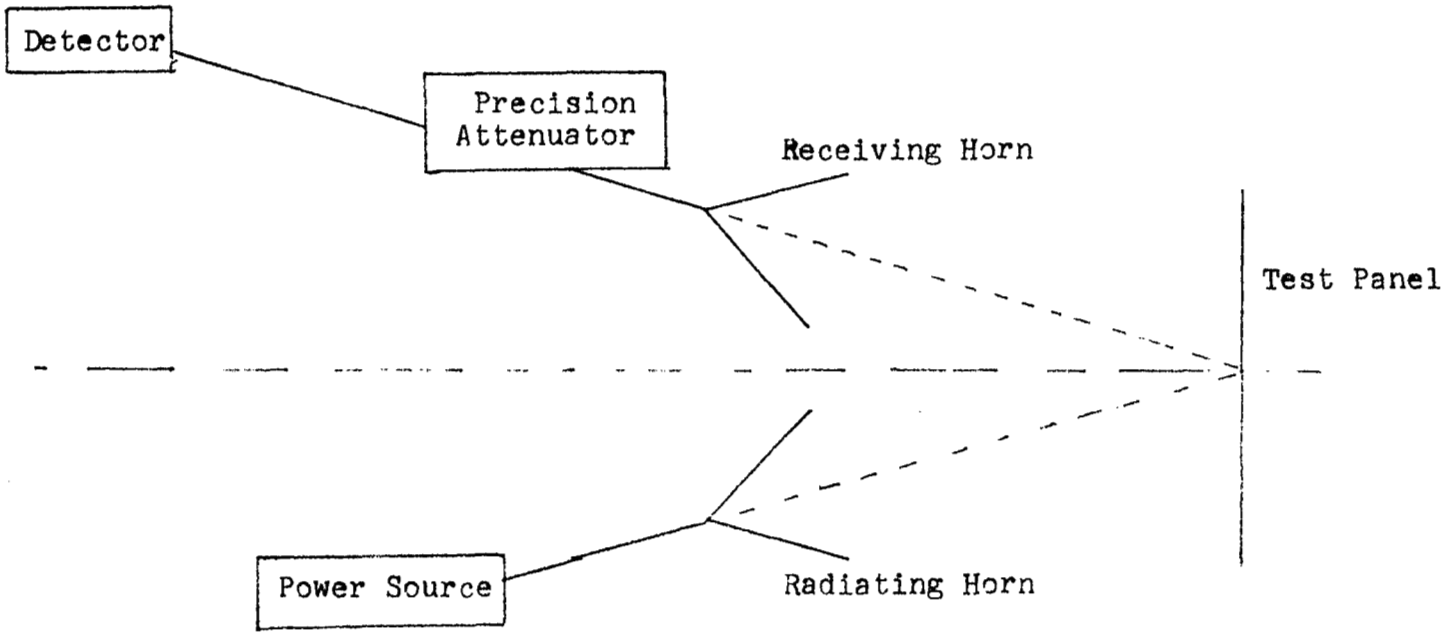

Figure 6. Transmitter-Receiver and Test Panel Arrangement

For an imperfect reflector with reflection coefficient Γ, the reflected power is

$$P_\Gamma = |\Gamma|^2 \frac{P_o G}{4\pi} \frac{A'}{2R^2}$$

Thus the ratio $P_\Gamma / P_r = |\Gamma|^2$ if the measurement is made under identical conditions. Comparison of the reflected powers in each case gives the power reflection coefficient $|\Gamma|^2$. A test on an array with long strips, which can be evaluated according to the inductive array of Appendix II, showed good agreement between the theoretical reflection coefficient and the value measured according to the above description.

3.3 Experimental Results for Array Reflection

The test arrays were made by adhering perfectly conductive metallic strips in regular patterns on a smooth surface of foam polystyrene. The foam polystyrene has a dielectric constant close to 1 and is equivalent to free space. The metallic strips are 1/16 inch wide and of negligible thickness. For all arrays the strips were parallel to each other and spaced with a periodicity of 1/4 inch. In the notation of Figure 5, $d' = 1/16$ inch, $a = 1/4$ inch. Each array differed from the others according to the values of A and D selected. Table 3 lists the array geometry and the reflection loss in each case. The reflection loss is the ratio of the reflected power in the main lobe for each array to that for the perfect reflector, expressed in db.

The case of an array of strips with no cuts or gaps has a reflection loss of 0.8 db as experimentally determined. As mentioned above, this is the same as that predicted theoretically from the equivalent circuit for the case of the infinitely long strips of the given geometry.

Figure 7 shows a plot of reflection loss versus strip length for various gap length arrays. The approach to the purely inductive strips with 0.8 db reflection loss can be seen for strips greater than 2λ. Furthermore, the rapid increase in reflection loss beyond strips equal to $\lambda/2$ can be noted. The special value of the strip equal to $\lambda/2$ seems to indicate a series resonance of the equivalent capacitance and inductance of the array elements. The shunt impedance of the array is thus zero and the reflected power increases. This is further discussed in the next section.

One of the results to notice is that if the gaps or what may be considered breaks in the conductive wires are small and the remaining lengths of wires are greater than a wavelength, only about 3 db reflection loss at most results. This is important in space

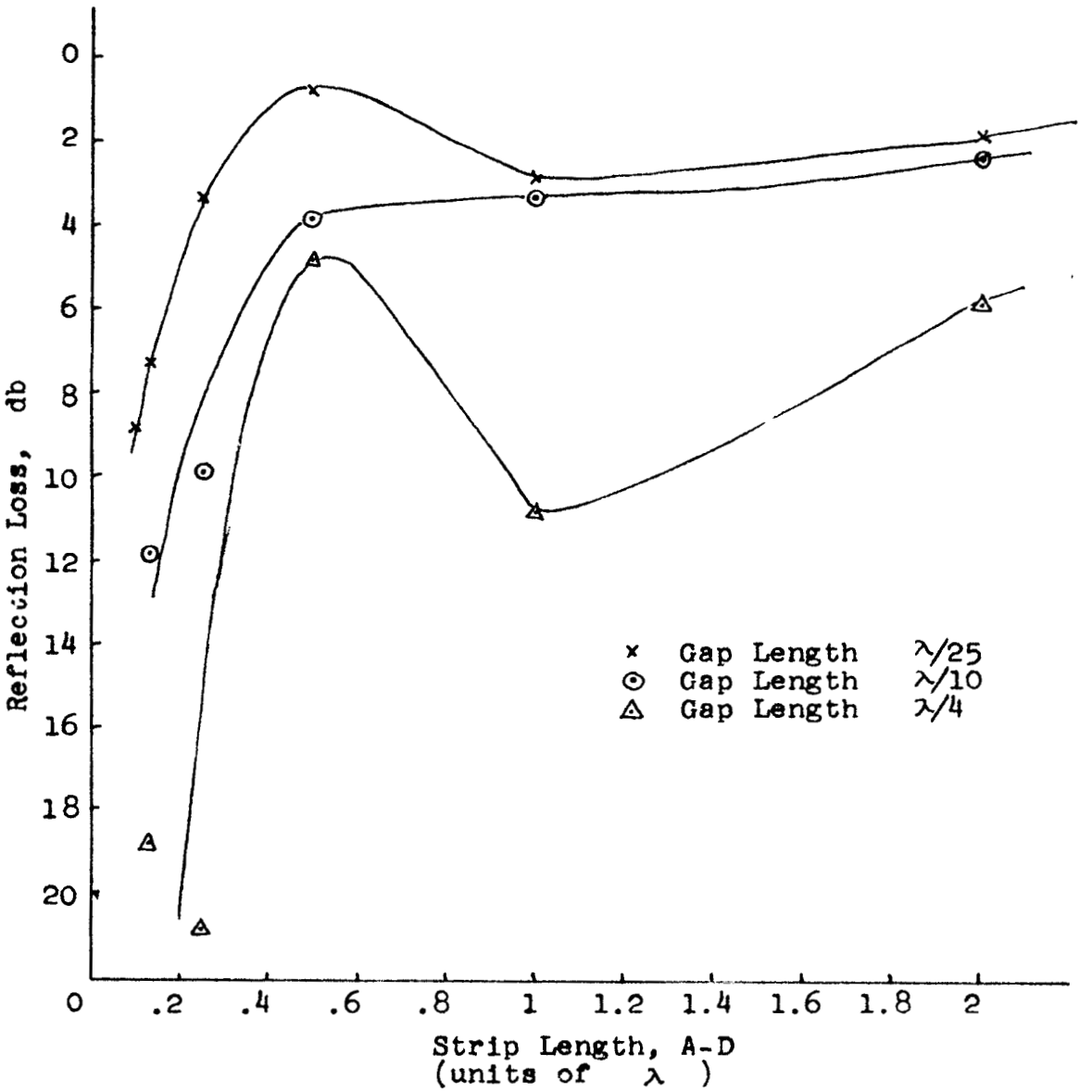

Figure 7. Reflection Loss versus Strip Length for Various Gap Lengths

Table 3

Reflection Loss for Test Panel Arrays

(Perfectly reflecting panel = 0 db)

Gap Length, D (multiples of λ)	Strip Length, A-D (multiples of λ)	Reflection Loss (db)
1/25	2	1.8
	1	2.8
	1/2	.8
	1/4	3.3
	1/8	7.3
	1/10	8.8
1/10	2	2.3
	1	3.3
	1/2	3.8
	1/4	9.8
	1/8	11.8
1/4	2	5.8
	1	10.8
	1/2	4.8
	1/4	20.8
	1/8	18.8
1/25	1	2.8
1/10		3.3
1/8		3.8
1/4		10.8
1/2		6.8

structure reflectors if one considers possible breaks occurring, or if the structure element size is limited because of erection design or other causes. For most practical purposes strip lengths larger than 2λ represent infinitely long strips.

Figure 8 is a plot of the reflection loss versus gap length for the one case of strip length equal to λ . As expected, reflection loss increases with gap length with a decrease however toward a gap length equal to $\lambda/2$.

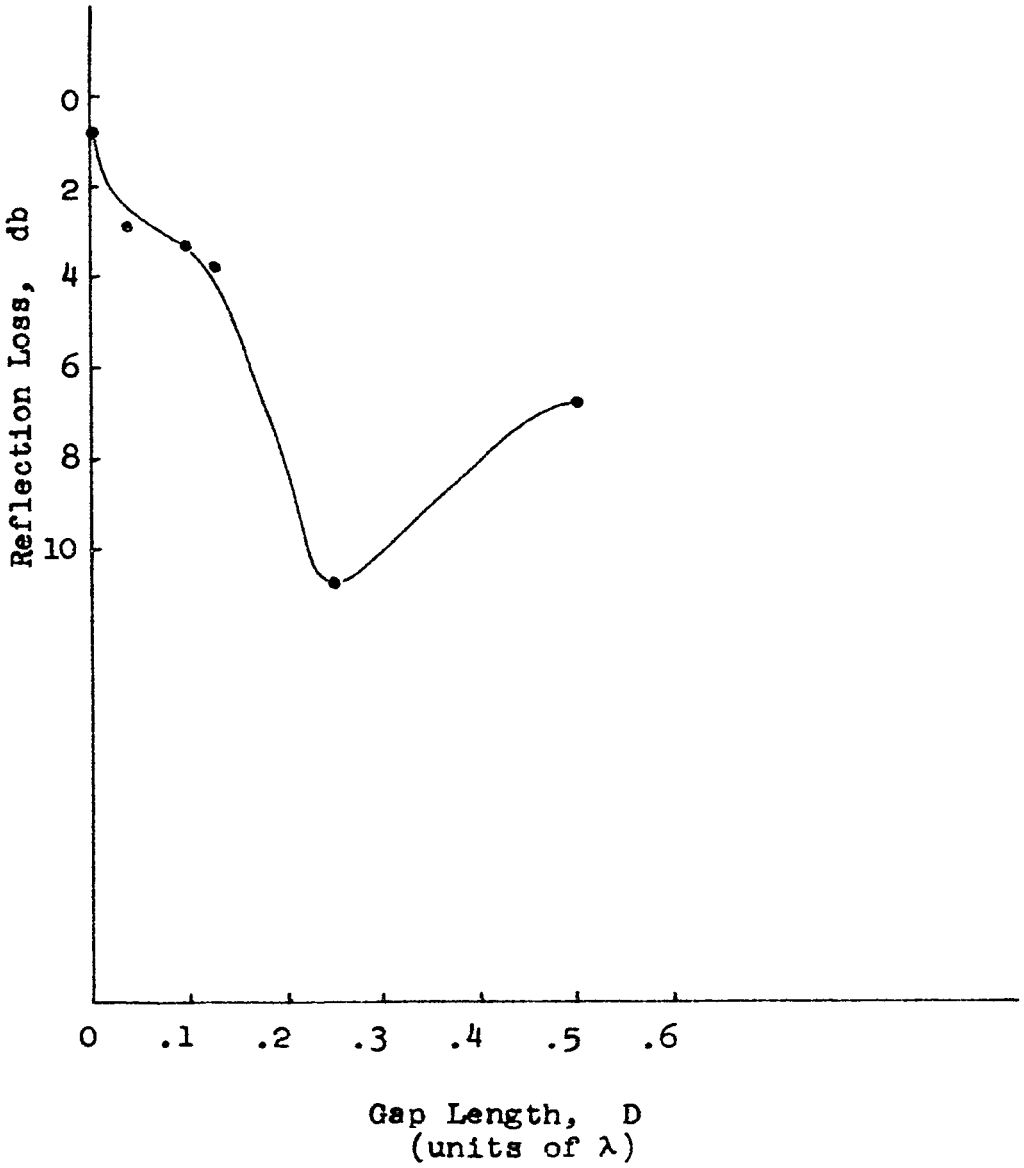

Figure 8. Reflection Loss versus Gap Length for Strip Length λ

3.4 The Equivalent Circuit of the Short Strip Planar Array

The effect of an element of a planar array in a microwave circuit can be described by means of its equivalent circuit. However, the circuit can be derived only in certain special cases many of which are given throughout the literature and in particular in the "Microwave Handbook"[8]. The planar array of the type discussed in this section is difficult to analyze. Nevertheless a qualitative estimate of the equivalent circuit can be given.

The planar array considered is the one shown in Figure 5. This is an array which has been formed from the infinitely long strip array with periodic gaps occurring in each strip. The strips are of infinitesimal thickness and therefore could be represented by an impedance shunting the transmission line for the TEM mode in free space. The strips are perfect conductors and the shunt impedance is lossless.

One limiting case of this problem is that in which the number of strips per wavelength is so large that one may take the circuit to be equivalent to the capacitive band of Case 2 in Appendix II. The capacitance is essentially that due to the gaps between the bands. The absence of portions of the bands, i.e., the sections of width a-d', might be accounted for by multiplying the capacitance of the full bands by the ratio of the missing sections of conductor and an additional factor to account for the resultant fringing fields, specifically $(d'/a)(\tau)$.

On the other hand the long strips (as the original long inductive strips) represent an equivalent inductance which is now changed because of the gaps of length D. If the inductance per unit length remained the same, then a corrective factor (A-D)/A could account for the reduced length of conductor. However, now because of the finite length of strips, currents at the ends cause somewhat different

current distributions in each isolated strip. Therefore, a correction factor $\frac{A-D}{A}\eta$ might be used.

An important consideration is the question of how both capacitance and inductance can be combined in the shunt impedance. One way of considering this is to examine the subdivided problem. This can then be connected with the dual problem for which a form of the equivalent circuit is known.

Each of the separate strips may be isolated from one another by inserting walls which do not alter the problem. These are electric walls perpendicular to the incident electric field and magnetic walls parallel to the electric field. Figure 9 indicates this subdivision where these walls have been chosen to isolate each individual strip in the center of the rectangular guide formed by the walls.

The strip in each guide is an iris. The dual of this problem is shown in Figure 10a, where E and H fields have been interchanged and the iris has become an aperture in a conducting plate. The aperture problem of Figure 10a has not been solved for the general case. However, the equivalent circuit suggested is as shown in Figure 10b,[9] which shows a shunt element of inductance and capacitance in parallel. Furthermore, it has been found empirically that the aperture is resonant for specific aperture ratios and where the long dimension is approximately half a wavelength.

Returning to the actual circuit, the equivalent circuit would be the dual of the shunt circuit in Figure 10b. This is shown in Figure 11. It is assumed that the corrected values of capacitance and inductance as described above can be used as the circuit elements.

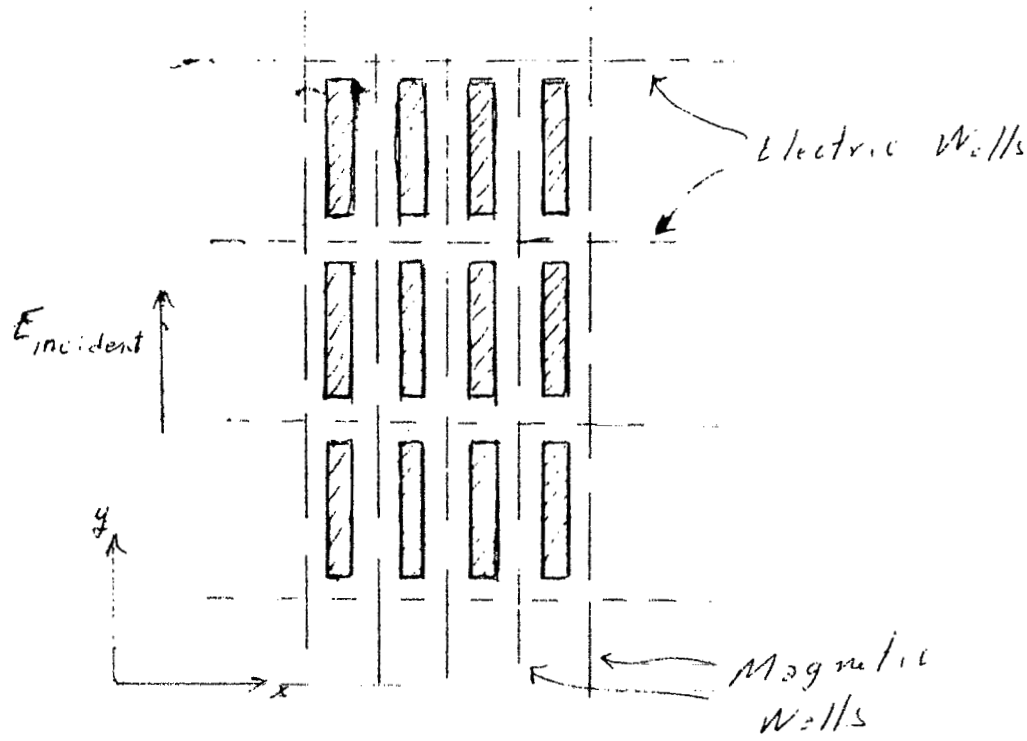

Figure 9. Array with Electric and Magnetic Walls Interposed

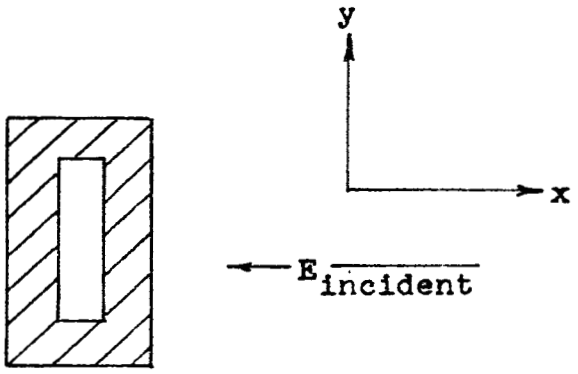

a. Dual Aperture to Iris of Figure 9

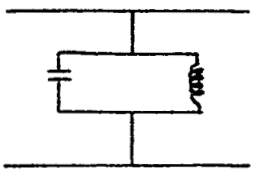

b. Equivalent Circuit

Figure 10

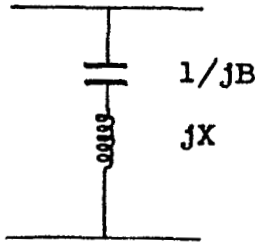

Figure 11. Proposed Equivalent Circuit for Short Strip Arrays

The circuit of Figure 11 has a normalized impedance

$$Z = \frac{1-BX}{jB}$$

and the power reflection coefficient is given by

$$|\Gamma|^2 = \frac{1}{1+4\left(\frac{1-BX}{B}\right)^2}$$

The resonance in the dual case at the iris length approximately half a wavelength now corresponds to the case $BX \rightarrow 1$ for which $|\Gamma|^2$ approaches 1. This should still be about the strip length $A-D \rightarrow \lambda/2$. The values of the elements are

$$B = \frac{4A}{\lambda}\left[\ln\left(\frac{2A}{\pi D}\right) + \frac{1}{2}\left(\frac{A}{\lambda}\right)^2\right]\frac{d'}{a}\,\tau$$

$$X = \frac{a}{\lambda}\left[\ln\left(\frac{2a}{\pi d'}\right) + \frac{1}{2}\left(\frac{a}{\lambda}\right)^2\right]\frac{A-D}{A}\,\eta$$

Certainly the result shows the correct type of variation. Thus as A becomes large and D small, B is large and the reflection reduces to that of the case for long inductive wires. Similar results hold for the other parameters, so that the decrease in reflection appears similar to that in Figure 7. Computations for some cases with the correction factors equal to 1 however indicate the resonant points closer to $A-D \simeq \lambda$. A value of η greater than 1 is required to bring this value closer to $\lambda/2$. Qualitatively this can represent the equivalent circuit.

SECTION 4
Thermal Radiation from Dust Distributions

4.1 The Dustwall as a Thermal Radiator

One of the promising applications of the dust space structure concept is the use of circulating dust streams as an efficient thermal radiator. The general concepts have been examined and analyzed in Reference 1. A number of points can be listed which make dust particles specially advantageous as thermal radiators. These are:

1. Large surface to mass ratio for the radiator units, resulting in a low total radiator system mass
2. Large space view factor with each particle of the dust radiator radiating essentially to outer space, unshadowed by other material
3. Choice of a radiator material is independent of the requirements imposed for a solid material with structural problems
4. General advantages of dust structures in space, such as freedom from meteoroid damage, etc.

This section describes an experimental measurement of the effectiveness of radiating dust particles in a region simulating space. The dust radiator is modeled by a stream of high-temperature dust particles falling by gravity from an oven. Temperature measurements are made both at the top and bottom of the particle drop path during which the particles have radiated to cold blackened walls. The temperature differences measured agree with the theoretical estimates according to radiation theory. For the length of drop of 8 inches, the temperature difference was 40°C for particles

initially at 800°C. The theoretical estimate was 80°C. This discrepancy can be explained as due to a number of factors which in reality would lower the theoretical value. For example, the emissivity of the dust particles used was taken at 0.8 as the handbook value at low temperatures. Other references indicate this can change greatly and give a value between 0,4 and 0.6 over a temperature range from room temperature up to 1300°K. If the value 0.6 were used then the theoretical temperature difference would be 65°C, a value closer to the measured one. This is further discussed in Section 4.5.

The fundamental equation for the dust radiator is that giving the initial and final temperatures of radiating dust. This was derived in Reference 1 and can be given as

$$T_d = \frac{T_o}{(1 + 3\alpha d\, T_o^3)^{1/3}}$$

where T_o is the initial dust temperature, T_d the final dust temperature, d the total path length, and α a parameter depending on particle properties and the radiative conditions. The parameter α is given by

$$\alpha = \frac{\sigma E A_s V_f}{m\, c_p\, v}$$

where A_s is the particle surface area ρ the dust particle material specific heat, m its mass, E the emissivity, σ the Stefan Boltzmann constant, v the particle velocity, and V_f the view factor. The optimum design for the radiator parameters has been discussed in the previously mentioned Reference 1. This relationship becomes the basic equation governing dust radiator

performance. The total heat radiated per gram of dust is given by $c_p \Delta T$ where ΔT is the temperature difference according to the above equation, i.e., $\Delta T = T_d - T_o$.

The experiments which are described here are designed to determine the important factor ΔT, verifying the general result given by this fundamental equation to within the experimental error. From the experiments one can therefore conclude that the dust radiator concept is verified.

In addition, experiments were conducted to determine the effective thermal conductivity of the dust in order to aid in the design of a dust oven. Because of the small contact area from particle to particle, the thermal conductivity of a pile of dust particles can be much smaller than that for the bulk material. The contact area varies with the force holding the particles together, the elastic properties of the particles, and their shape. Dependent upon these quantities, the effective conductivity of a pile of dust particles may be reduced one or more orders of magnitude from that for the bulk material. The experiments conducted showed that the specific particles considered here had a reduction factor which was about 20. This factor includes the effect of transfer of heat through physical contact, as well as radiation across gaps between particles.

4.2 The Test Radiator Experiment

The purpose of the experiment is to model a radiator device with a high-temperature dust stream moving through a region simulating deep space, and to measure its thermal radiation.

The dust is heated in an oven specifically designed and built to operate within a vacuum envelope and to heat dust flowing continuously through it. At a temperature of about 1000°C the particles are emitted from the oven exit port. Falling under gravity, the particles form a dust stream which is surrounded by a blackened, cooled cylinder. At the end of its fall, the material is received by a collector. Figure 12 shows a schematic view of this system. The important parameter to measure is the difference in dust stream temperature at emission from that at its entry to the collector, as a function of the total path length during which radiation occurs. The experiment is performed in vacuum of about 10^{-6} torr at which pressures, gas thermal conductivity, particle oxidation, windage, and air resistance are not problems. The overall vacuum envelope is a glass bell jar, 18 inches in diameter. The material used throughout most of the experiments was graphite powder, which varied in size from 50 microns to about 200 microns.

Dust temperature measurement was made by using two optical pyrometer strips built directly into the system itself, at the top and bottom of the dust drop space. These strips were heated by passing electric current through them until the resultant color matched that of the hot dust passing before them. At this temperature, the dust particles were not visible against the background of the pyrometer strips. The pyrometer temperature itself was measured with small thermocouple leads attached directly to the strips.

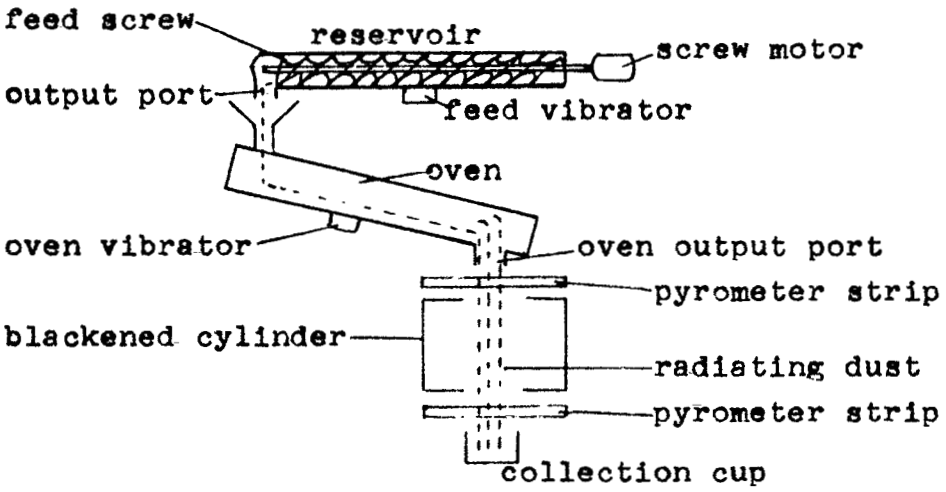

Figure 12. Schematic Dust Oven-Radiator System (Entire System Enclosed Within Vacuum Envelope)

4.3 Range of Parameters of the Test Radiator

The design of the system depends critically on the range of parameters to be expected. These parameters are the quantities in the equation for the dust temperature as given in Section 4.1. That equation is based on a number of assumptions which should be noted. In addition the choice of the constants involve certain approximations as well.

First, the particle velocity has been assumed to be constant during the radiation path. This would be true in a space system but is not so in the laboratory experiment as designed. For this case, v has been taken as the average velocity over the total path.

A second assumption involves the value selected for the emissivity of the particles, taken to be that for the bulk material. This assumes the material to be opaque. However, if the particle size becomes small enough, and espcially in the case of non-metals for which the absorptance may not be high, the transmittance becomes important.[9] Normally the emittance for any material has a value different from that for a black body due to the surface reflectance. Thus the relationship $E+R=1$ holds for opaque bodies where E is the emittance and R the reflectance. With non-opaque bodies (those sufficiently thin to transmit some of the energy) the relationship is $E+R+T=1$ where T is the transmittance. Thus E in this case becomes smaller than that for an opaque body. A particle of micron size range may be small enough to have an effective emittance less than that for the bulk material. Use of the opaque material emittance value in the equations therefore will predict a higher temperature difference than may actually be the case.

The value of the view factor V_f can be taken as 1. Except for extremely high dust densities, which are not of interest here, computations can show that this factor is unity.

The standard particle here is to be considered a sphere for which the area and mass per particle can be determined. However, in most cases dust particles are found to be discs or platelets of irregular shape with a larger surface area to mass ratio than the sphere.

The derivation of the equation for the final temperature T_d assumes the dust to be radiating to a 0° K environment from an initially high temperature range. Exact calculations show that for the parameters of interest, say where $T_o = 1000^\circ C$, an error of less than 5% results between $0^\circ K$ and a background of room temperature. With these considerations in mind, the temperature T_d has been computed for a number of cases pertinent to the laboratory test. This is shown in the graph of Figure 13, which shows temperature difference versus spherical particle diameter for initial temperatures of $800^\circ C$ and $1000^\circ C$. Here the velocity v is chosen as $2/3\sqrt{2gd}$ where g is the acceleration due to gravity and d the total radiative path length, corresponding to the average velocity with an initial zero velocity on emergence from the oven. For $d = 20$ cm, as is the case in the experiment, $v = 130$ cm/sec. Table 4 lists the particle parameters chosen.

Table 4

Parameters for Dust Radiator Experiment

Material: Powdered Graphite
Diameter: 50 to 200 microns
Specific Heat; c_p: .25 at $100^\circ C$, .45 at $1000^\circ C$ (cal/gm $^\circ C$)
Emissivity, $E = 0.8$
Bulk Material Density, ρ 2.25 gm/cm^3
View Factor, $V_f = 1$
Total Path Length, $d = 20$ cm

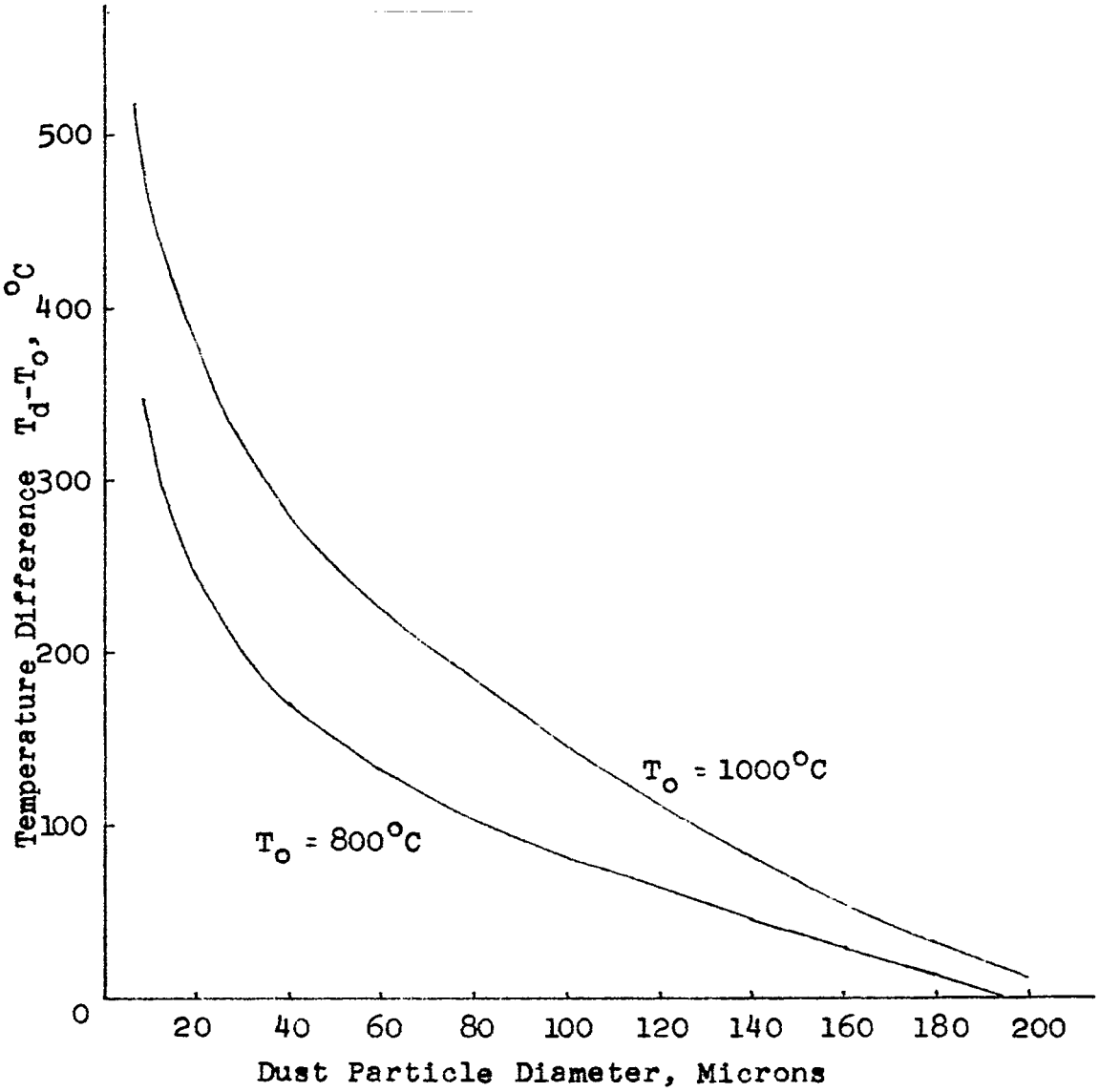

Figure 13. Temperature Difference Due to Thermal Radiation versus Particle Diameter

These values lead to a parameter value $\alpha d = 1.0 \times 10^{-9}/(^{\circ}K)^3$ for a particle diameter of 10 microns up to a value of $1.0 \times 10^{-10}/(^{\circ}K)^3$ at a particle diameter of 100 microns.

It can be seen than that the expected temperature difference would be of the order of 100°C for particles in the 100 micron range. The experiments described in this section were designed to measure this temperature difference.

4.4 Heating of Dust in a Vacuum Oven

One of the important parameters for the design of a vacuum dust oven is the effective thermal transfer for collective dust particles in contact. Here only two mechanisms may be of importance; direct thermal conductivity through the small particle contacts or radiation across open gaps from one particle to its visible neighbors. The question of which of these two competing processes is the major one depends upon such factors as local average particle temperatures, bulk material properties such as conductivity and emittance, as well as the areas involved in each case. An estimate of the relative importance can be made as follows:

If one assumes that the temperature difference between neighboring particles is not large, as would actually be the case, then the radiation expression can be linearized so that the thermal flux due to radiation will be $5.5 \times 10^{-4}\ E A_r T_a^3\ \Delta T$ cal/sec where T_a is the average temperature, A_r the effective radiating area, and ΔT the temperature difference of the particles involved.

On the other hand, the heat flux by direct conduction across the small contact area between neighboring particles is given by $2Ka\ \Delta T$ cal/sec where K is thermal bulk conductivity and a the radius of the contact area. This is derived assuming the contact area is so small that one may compute the thermal resistance as that due to the transfer from one semi-infinite body into another through a common circular area of radius a.[11] As a rough estimate, assume the contact area is approximately 1/100 the particle area. Using the parameters of Table 4 for graphite, and for which $K = .012$ cal cm/sec ^{o}C, then the ratio of the radiation flux F_r to the conduction flux F_k is

$$\frac{F_r}{F_k} = \frac{5.5 \times 10^{-4}\ E\ A_r\ T_a^3}{2K\ a} \approx 2 \times 10^{-2}\ \frac{A_r}{a}\ T_a^3$$

For a 50 micron diameter particle, for which $A_r \approx 8 \times 10^{-5}$ cm^2 and for the case chosen $a \approx 5 \times 10^{-4}$ cm, then

$$\frac{F_r}{F_k} = 3 \times 10^{-3} T_a^3$$

Thus even for room temperatures the radiation flux is much larger than the conduction flow.

Nevertheless, no matter which mechanism is the important one, since layers of neighboring particles will be close in temperature, both mechanisms result in a flux proportional to the temperature difference between neighboring layers of particles. We may then define an overall effective thermal conductivity factor γ, such that the flux is given by $\gamma \Delta T$.

An experimental oven was constructed and the effective particle conductivity was determined with its use. Figure 14 shows a diagram of the oven. This oven, as well as the oven used for the radiation test, was made with a machinable ceramic,* an alumino-silicate which can be hardened by firing with a prescribed heat process. The radiation test oven is shown in Figure 15.

A charge of 3 grams of graphite powder filled the inner cup. Thermocouples placed as shown monitored the powder temperature at the center and at the outer edge. With the heater cup kept at 1000° C, the temperature increase of the dust was noted for approximately 30 minutes. Table 5 gives the measured values of the dust temperatures as well as the ratio for the two positions.

* Aremcolox grade 502-1100, Aremco Products, Inc.

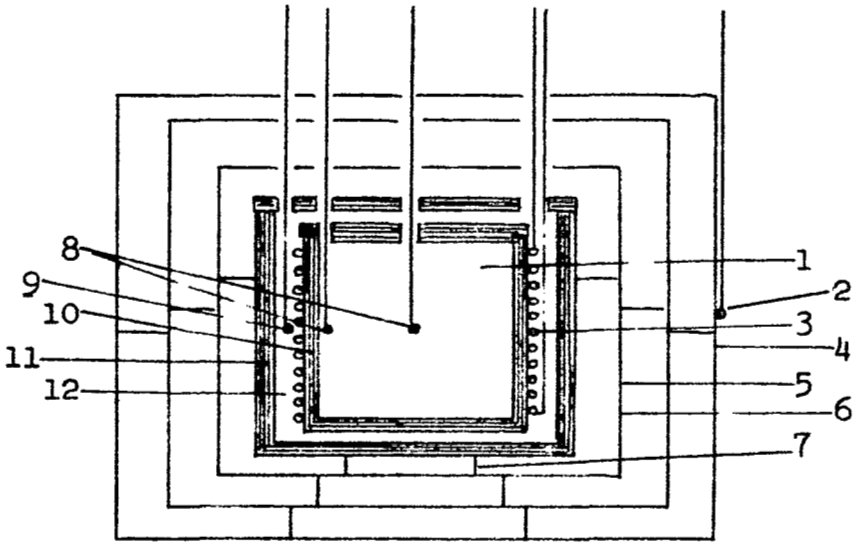

LEGEND

1	graphite powder	7	shield supports
2	heat shield thermocouple	8	powder thermocouples
3	heating filament, 10-mil tungsten	9	filament thermocouple
4	outer heat shield	10	inner ceramic cup
5	center heat shield	11	outer ceramic cup
6	inner heat shield	12	Alundum powder

Figure 14. Cross Section Through Oven Used for Determining Heat Transfer in Static Pile of Graphite Particles in Vacuum

(Dimensions on following page)

DIMENSIONS

Inner Cup:

overall height	1.06 "
inside height	.935"
outside diameter	.985"
wall thickness	1/16"
filament windings	22 turns per inch 20 loops total

Outer Cup:

overall height	1.31"
outside diameter	1.37"
wall thickness	1/16"

Inner Heat Shield:

outside diameter	1-7/8"
height	2"
material	stainless steel, type 302, 5 mils thick

Center Heat Shield:

outside diameter	2-3/8"
height	2-1/2"
material	stainless steel, type 302, 5 mils thick

Outer Heat Shield:

outside diameter	2-7/8"
height	3"
material	stainless steel, type 302, 5 mils thick

Figure 14. (Continued)

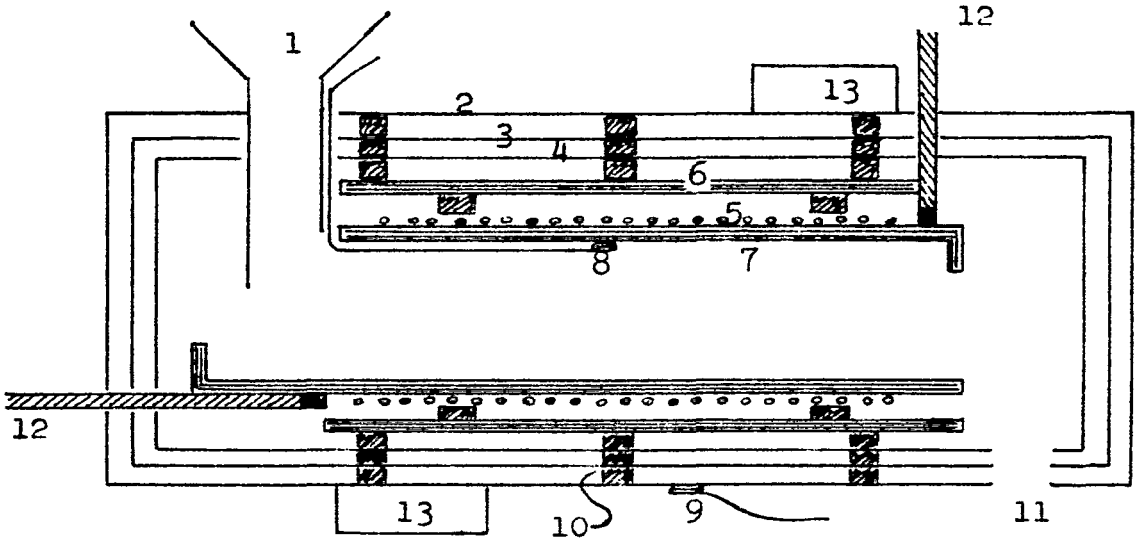

LEGEND

1	feed funnel	7	inner (oven) ceramic tube
2	outer shield	8	inner (oven) thermocouple
3	center shield	9	outer (shield) thermocouple
4	inner shield	10	ceramic spacers
5	parallel heater windings	11	output port
6	outer ceramic tube	12	nickel ring and power connection to windings
		13	vibrators

Figure 15. Longitudinal Cross Section Through Dust Radiator System Oven

(dimensions on following page)

DIMENSIONS

Inner Ceramic Oven Tube:

inside diameter	.770"
outside diameter	.875"
overall length	6-5/8"
heater winding length	5-1/4"

Outer Ceramic Tube:

inside diameter	1.085"
outside diameter	1.2"
overall length	6"

Inner Shield:

diameter	1.3"

Center Shield:

diameter	1.57"

Outer Shield:

diameter	1.87"

Figure 15. (Continued)

Table 5

Temperatures Measured in Heat Transfer Test for Graphite Powder

Time of Heating (min)	Temperature at Edge (°C)	Temperature at Center (°C)	Center Temperature / Edge Temperature
3	440	380	.865
10	760	690	.905
15	880	800	.910
20	950	890	.935
30	1010	940	.933

If one considers a cylinder whose outer edge is kept at constant temperature (e.g. the 1000°C of the ceramic cup) and the initial temperature of the cylinder of dust is zero, then the solution of the conduction problem through the dust cylinder can be given in terms of a parameter $(K/\rho c_p)(t/a^2)$ where K is the effective thermal conductivity of the dust cylinder, ρ its density, c_p the specific heat, a the cylinder radius, and t the time.[11]. Here the conductivity will be the linear proportionality factor γ which accounts for both contact conductivity and radiation from particle to particle as well as conductivity through the particle itself. The solution is given in graphical form by Carslaw and Jaeger, page 200. From that chart the values of diffusivity $\kappa = K/\rho c_p$ can be found, from which one can compute the quantity K or as it would be used here, γ. This is given in Table 6.

Table 6

Diffusivity and Conductivity as Determined from Carslaw and Jaeger

t (min)	$\frac{\kappa t}{a^2}$	κ $\frac{cm^2}{sec}$	$K = \tau$ $\frac{cal\ cm}{cm^2\ sec\ ^oC}$
3	.45	.0025	.0005
10	.50	.0008	.00014
15	.52	.00058	.0001
20	.54	.00048	.0001
30	.54	.0003	.00005

The handbook value for bulk thermal conductivity of graphite is given as .012 cal cm/cm^2 sec ^oC at room temperature. Here the first entry in the table would give a value of τ at 1/20 to 1/100 that for the bulk material. This value can then be used in the design of the oven for static particles, replacing the dust with an equivalent material with this conductivity. It should be noted that rough theoretical estimates of dust conductivity for conduction alone would give a value of the order 1/100 the bulk value for this case. A discussion of the reduction of conductivity due to particle contact is given in Appendix III.

If radiation is the main mechanism of heat transfer between particles, the factor τ should vary as temperature cubed. From the lowest temperature to the highest noted, this is a factor of six. However, the experimentally-determined factor seems to decrease by a factor of five. This may be due to the decrease in thermal conductivity of the bulk material which also affects the overall proportionality constant τ.

4.5 The Experimental Radiator System and Results

As described in Section 4.2, the dust radiator was simulated by a model in which powdered material was heated and subsequently dropped by gravity through a space-simulating region. The overall system has been shown in Figure 12.

The oven is a tubular ceramic vessel made of two coaxial cylinders with three stainless steel heat shields. This is shown in Figures 15, 16A, 16B and 16C. Dust flows into the inner cylinder at one end and out its opposite end. This flow is brought about by vibration and gravity, with the oven positioned at 10° to 20° with respect to the horizontal.

The outer surface of the inner cylinder is wound with 5 parallel rows of 10-mil tungsten wire, 4 turns per inch, each laid in a groove machined in the cylinder surface and held in place by a thermally-conductive cement. The total heater resistance was .32 ohm at room temperature and 3.2 ohms at the high 1000°C temperature.

The oven was brought up to temperature with no dust flow, after which the material was forced through at a rate of .2 gram/sec. The total powder charge held in the reservoir was 80 grams. Oven input remained at 300 watts during the dust flow. The total length of the oven is 6 inches. This is adequate to bring the dust at the given flow rate to an exit temperature above 800°C.

Upon departure from the oven, the material formed a rectangular stream approximately 1/4 inch by 3/4 inch and fell a distance of 25 cm to the collector. At an interval spacing of 20 cm along this path the optical pyrometer strips measured dust temperature. These are well-oxidized nichrome resistance strips whose emittance would be 0.8, the same as graphite.

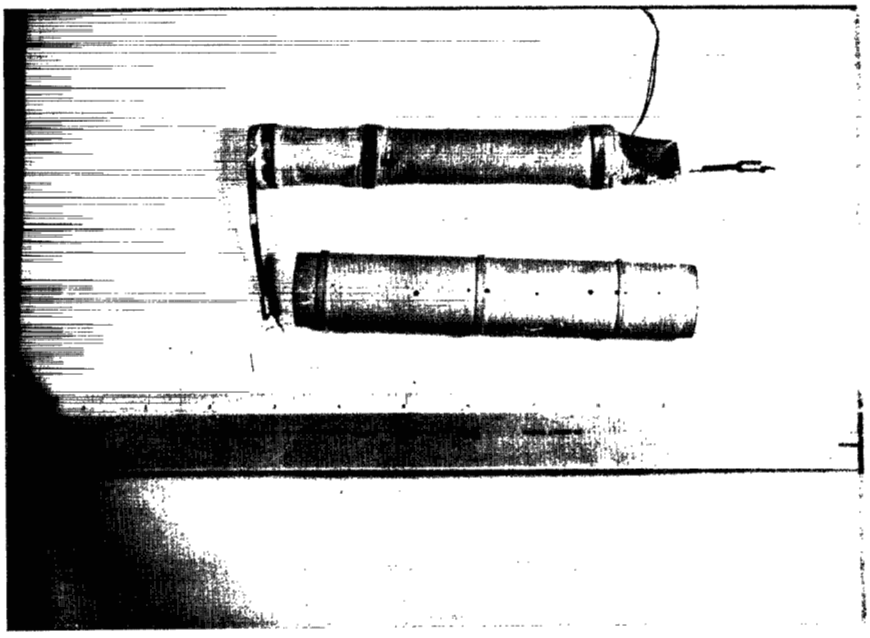

Figure 16A. Upper: Inner Ceramic Oven Tube
Lower: Outer Ceramic Tube

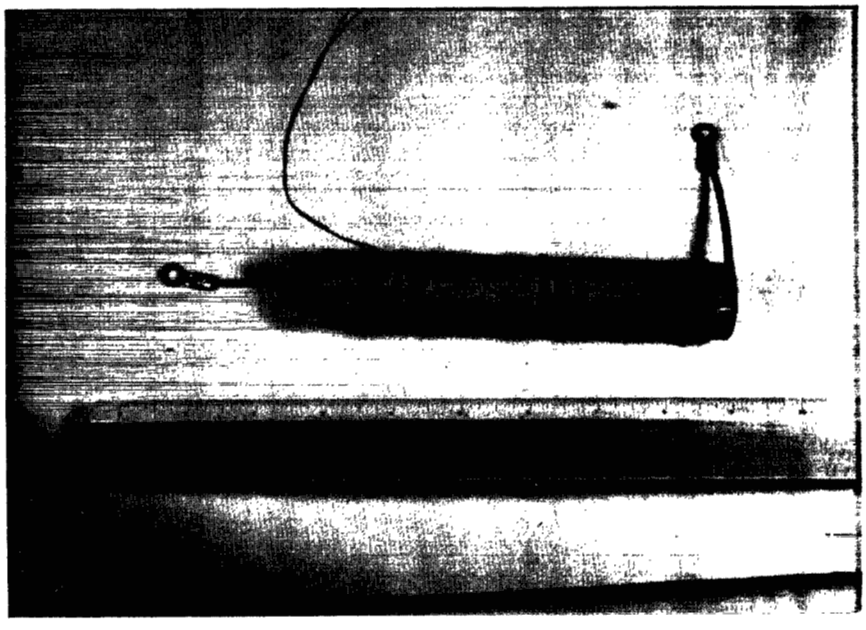

Figure 16B. Inner and Outer Ceramic Tubes Assembled
Winding and oven thermocouple lead wires can be seen.

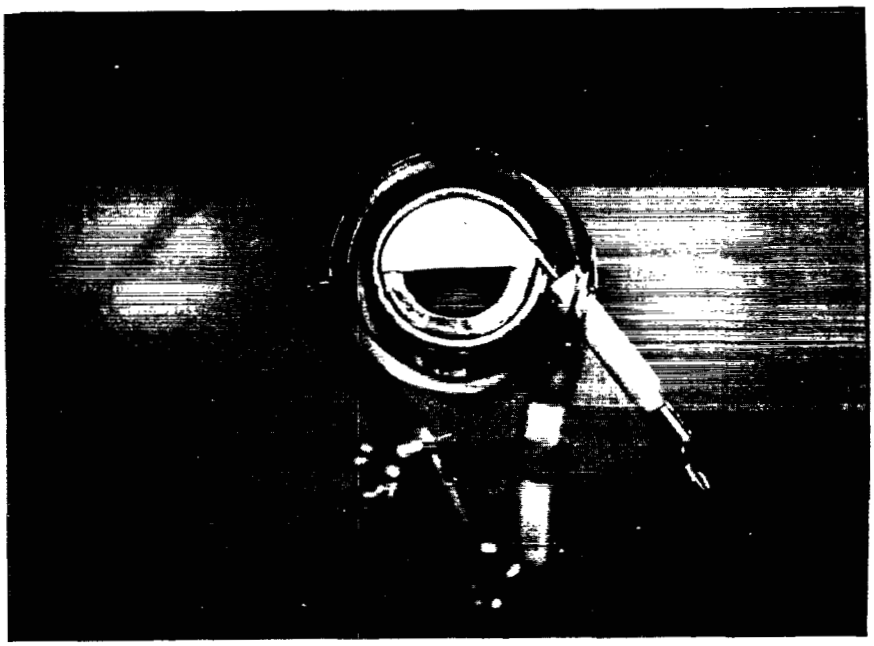

Figure 16C. Output End of Oven Shown With End Shield Caps Removed

The three heat shields with ceramic spacers and the two inner concentric ceramic cylinders can be seen. One of the winding leads protrudes.

Figure 17 shows the oven in position and one of the pyrometer strips below it. The reservoir tube and the funnel leading from it into the oven can also be seen. Figure 18 shows the bright-hot dust stream as it passes the optical pyrometer.

Dust temperatures were measured repeatedly for the graphite powder. Table 7 gives the results for several of the runs.

Table 7

Temperature Readings for Several Graphite Powder Drops

Upper Pyrometer (°C)	Lower Pyrometer (°C)	Temperature Difference $T_o - T_d$ (°C)
800°	760	40
825	775	50
900	840	60

Size distribution of the graphite particles used in the experiments is given in Table 8.

Table 8

Size Distribution of Powdered Graphite Particles Used in the Experiments

Diameter Size Range (microns)	Average Diameter (microns)	Ratio by Weight	Theoretical Temperature Difference (T_o = 800° C)
177 to 234	205	.02	0
140 to 177	158	.03	35
104 to 140	122	.19	65
74 to 144	107	.25	80
44 to 140	92	.51	90

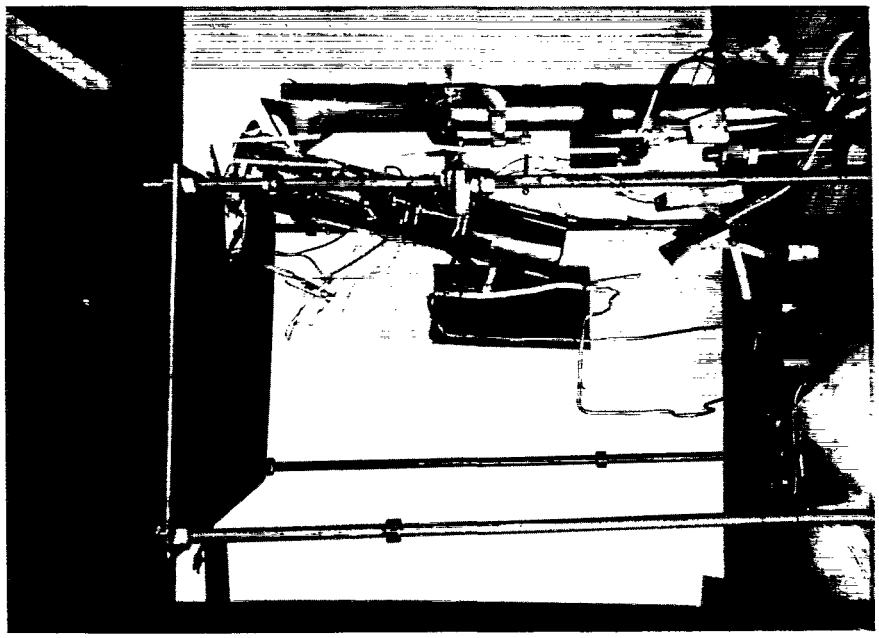

Figure 17. The Radiator System

This view shows the shielded oven, input funnel, feed reservoir, electrical connections, and supports. An optical pyrometer at red heat can be seen in front of the black rectangle at center. The vacuum envelope has been removed.

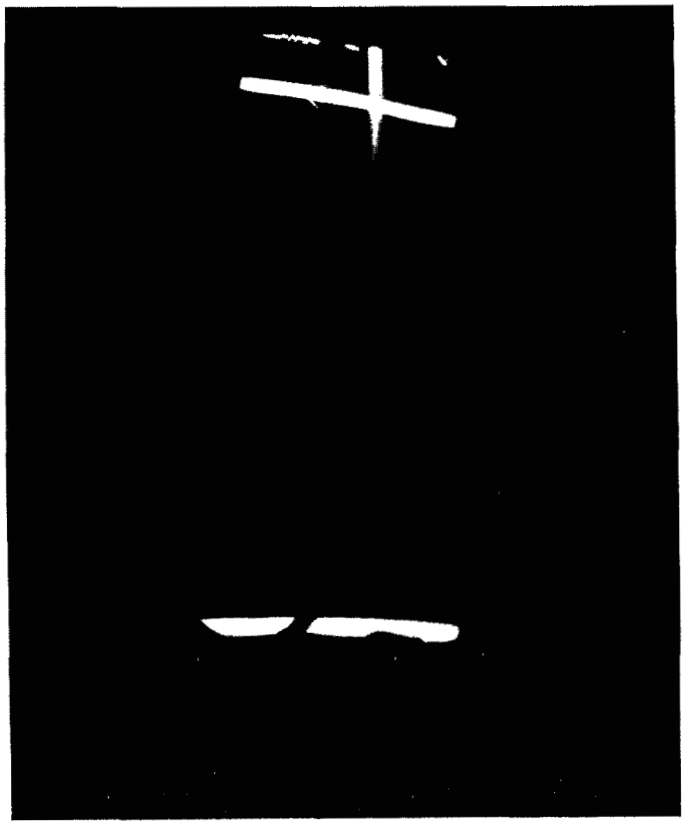

Figure 18. The Dust Stream Passing the Upper Optical Pyrometer Strip

The lower pyrometer strip can also be seen but this exposure was too short for dust to be seen at that level.

A weighted average of the expected temperature would be about $79^{\circ}C$ if $800^{\circ}C$ is the initial dust temperature. The measured value was $40^{\circ}C$. This discrepancy may be due to two important factors: First, the exact value of emissivity is not known but has been taken from the handbook values. However, other published data[12] shows values of total emissivity for graphite between $300^{\circ}K$ and $1400^{\circ}K$ to be .4 to .6. If this lower value of emissivity were true, then the theoretical difference temperature should be lower than the $80^{\circ}C$. It should be noted that since the temperature varied over a small range the emissivity would be fairly constant and the measured difference would be independent of the emissivity. A value of emissivity of 0.6 would theoretically reduce the 80° to 65°.

A second factor which would lower the temperature difference is the actual transit time during radiation. For the purpose of calculations this is taken as corresponding to the average velocity in falling under gravity starting from rest. In the experiment, on ejection of particles from the oven, an initial particle velocity was required, reducing the transit time and the amount of radiation.

It is evident that within the range of the known parameters the experiment agrees fairly well with theory.

APPENDIX I

The Dielectric Constant of Particles Embedded in a Dielectric Medium

The relationship between the equivalent dielectric constant for the dust distribution embedded in a dielectric medium can be derived as follows. Let ε be the medium dielectric constant, E the electric field, P the polarization, and E' the effective field acting on a small elemental volume surrounded by all the other dipoles. If $N\alpha$ is the dust dipole polarizability per unit volume, one can write for the total polarization

$$P = P_{dielectric} + P_{dust}$$

$$= \frac{\varepsilon - 1}{4\pi} E + N\alpha E'$$

But E' can also be written as

$$E' = E + \frac{4\pi}{3} P$$

Eliminating E' from the two equations gives

$$P = E \frac{N\alpha + \frac{\varepsilon - 1}{4\pi}}{1 - \frac{4\pi}{3} N\alpha} = \eta E$$

The new dielectric constant ε' is given by

$$\varepsilon' = 1 + 4\pi\eta$$

which gives

$$\varepsilon' = \frac{\varepsilon + \frac{8\pi}{3} N\alpha}{1 - \frac{4\pi}{3} N\alpha}$$

But α as given here is the polarizability of a particle embedded in the dielectric of the carrier medium. Thus $\alpha = \varepsilon a^3$ where a is the radius of the spherical particle. Inserting this in the formula above gives the final result

$$\varepsilon' = \frac{\varepsilon + \frac{8\pi}{3} Na^3\varepsilon}{1 - \frac{4\pi}{3} Na^3\varepsilon}$$

APPENDIX II

The Equivalent Circuit of Inductive and Capacitive Long Strip Arrays

The equivalent circuits for periodic arrays of parallel conductors have been given in the Waveguide Handbook. Two cases for infinitely thin strips are presented here.

a. The Inductive Case

This is the case of strips parallel to the incident E field as shown in the diagram below.

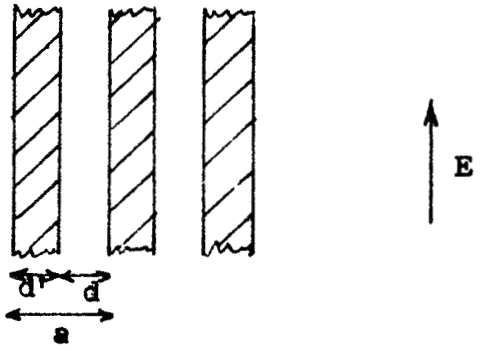

Inductive Strips

For normal incidence the equivalent circuit for this situation is given as a shunt inductance:

$$\frac{X}{Z_o} \approx \frac{a}{\lambda}\left[\ln\left(\frac{2a}{\pi d'}\right) + \frac{1}{2}\left(\frac{a}{\lambda}\right)^2\right]$$

for $d'/a << 1$ and $a/\lambda << 1$. Z_o is the characteristic impedance of free space and λ the free space wavelength. The equivalent circuit is shown below at the plane of the strips.

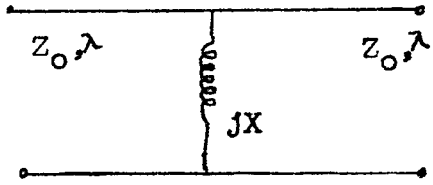

Equivalent Circuit for Inductive Strips

b. The Capacitive Case

This is the case of strips perpendicular to the incident E field as shown in the following diagram:

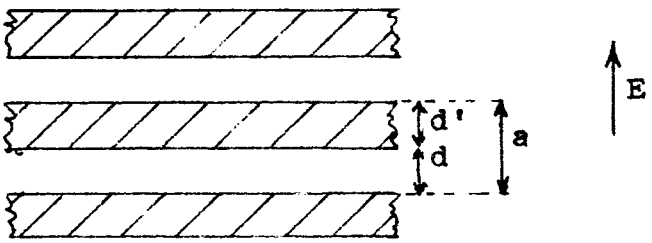

Capacitive Strips

For normal incidence the equivalent circuit is given as an admittance jB whose value is given by

$$\frac{B}{Y_o} = \frac{4a}{\lambda_o}\left[\ln\left(\frac{2a}{\pi d}\right) + \frac{1}{2}\left(\frac{a}{\lambda}\right)^2\right]$$

for $d/a << 1$ and $a/\lambda << 1$. Y_o is the characteristic admittance of free space and λ the free space wavelength. The equivalent circuit is shown below at the plane of the strips.

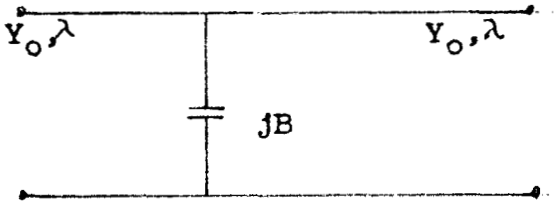

Equivalent Circuit for Capacitive Strips

APPENDIX III

Effective Thermal Resistivity of a Bed of Particles

Heat transfer by conduction takes place in a bed of particles through the points of contact of the particles and is critically dependent upon the total area of contact. (Additional transfer may occur due to thermal radiation.) The contact area will be dependent upon particle material and its characteristics such as Young's modulus, shape, size, uniformity of particles, forces holding particles together, etc. We can estimate the conductivity and show that the bulk conductivity can easily change from the solid material conductivity by an order of magnitude or more in some cases.

Let us specialize to a bed of uniform size, spherical particles of radius r and an area of particle contact at a single contact point given by πa^2 with $a \ll r$. Then the flow of heat into the particle through the contact point is the same as that into a semi-infinite slab over an input circle of radius a. For such a case, the thermal resistance is

$$R = \frac{1}{4ka}$$

where k is the thermal conductivity of the solid material; $k = 1/\rho$ where ρ is the thermal resistivity. For two particles in contact with one another over this contact area heat has to flow out of one particle through the contact area and into the second particle by a similar process. Thus for two particles in contact, the contact resistances are in series and

$$R = \frac{1}{2ka}$$

If a particle is in contact with a base plate of conductivity k_b, then the total resistance is

$$R = \frac{1}{4k_b a} + \frac{1}{4ka} = \frac{1}{4a}\left(\frac{1}{k_b} + \frac{1}{k}\right)$$

Now consider the heat flow problem to be a one-dimensional one so that lateral heat flow does not occur. Thus laterally adjacent particles are at the same temperature, and side contacts are of no importance for heat flow. Further consider particles to be stacked in the direction of heat flow, like beads on a string. (Closely-packed spheres would give a slightly different result but such differences are of little importance here.) As a result there are $1/2r$ particles per unit length and therefore $1/2r$ contacts in series over a unit length. The resistance per unit length is

$$\frac{R}{\text{unit length}} = \frac{1}{8kar}$$

But the resistance of a cylinder of radius r of solid material is $\rho/\pi r^2$. Therefore writing for the particle column

$$R = \frac{\rho_a}{\pi a^2}$$

where ρ_a is the apparent resistivity and equating both expressions,

$$\rho_a = \rho \frac{\pi r}{8a}$$

Estimates for typical materials and for a pressure holding the particles together of the order of the force of gravity give values of $r/a \approx 100$ to 1000. This results in a conductivity decrease by a factor of the order of 30 to 300.

LITERATURE CITED

1. Klahr, C.N., Cutler, S.N., Kalikstein, K., "Application of Dust for Space Structures", NASA-CR-1136, Aug. 1968
2. Ragan, G.L., "Microwave Transmission Circuits", MIT Radiation Laboratory Series, McGraw Hill, Inc., New York. 1948
3. Von Hippel, "Dielectric Materials and Applications", John Wiley & Sons, Inc., New York 1954
4. Van de Hulst, H.C., "Light Scattering by Small Particles", John Wiley & Sons, Inc., New York 1962
5. Silver, S., "Microwave Antenna Theory and Design", MIT Radiation Laboratory Series, McGraw Hill, Inc. New York, 1949
6. Becker, R.C., Coleman, P.D., "The Dielectric Tube Resonator: A Device for the Generation and Measurement of Millimeter and Submillimeter Waves", Proceedings Microwave Research Institute Symposia Series, Vol. IX, Millimeter Waves, Polytechnic Institute Press, New York, 1959
7. Schineller, E.R., Heinemann, H.M., Wilmot, D.W., Redlien, H.W., "Development of Macroscopic Waveguide and Waveguide Components for Optical Systems", NASA CR-332, Jan. 1966
8. Marcuvitz, N., "Waveguide Handbook", MIT Radiation Laboratory Series, McGraw Hill, Inc. New York, 1951
9. Montgomery, C.G., Dicke, R.H., Purcell, E.M., "Principles of Microwave Circuits", MIT Radiation Laboratory Series, McGraw Hill, Inc. New York 1948
10. Harrison, W., "Pitfalls in Thermal Emission Studies, Measurement of Thermal Radiation Properties of Solids" NASA SP-31, 1963
11. Carslaw, H.S., Jaeger, J.C., "Conduction of Heat in Solids", Oxford University Press, London, 1959
12. Siegel, R., Howell, J.R., "Thermal Radiation Heat Transfer", Vol. I, NASA SP-164, 1968

NASA-Langley, 1970 —— 33 CR-1530